Development Of Reservoir Characterization Techniques And Production Models For Exploiting Naturally Fractured Reservoirs

Final Technical Report
Project Period
July 1, 1999 through December 24, 2002

Incorporating the Semiannual Technical Progress Report
for the Period July 1, 2002 through December 24, 2002

Principal Authors
Michael L. Wiggins, Raymon L. Brown,
Faruk Civan, and Richard G. Hughes

December 2002

DE-AC26-99BC15212

The University of Oklahoma
Office of Research Administration
1000 Asp Avenue, Suite 314
Norman, OK 73019

DISCLAIMER

Abstract

Development Of Reservoir Characterization Techniques And Production Models For Exploiting Naturally Fractured Reservoirs

For many years, geoscientists and engineers have undertaken research to characterize naturally fractured reservoirs. Geoscientists have focused on understanding the process of fracturing and the subsequent measurement and description of fracture characteristics. Engineers have concentrated on the fluid flow behavior in the fracture-porous media system and the development of models to predict the hydrocarbon production from these complex systems. This research attempts to integrate these two complementary views to develop a quantitative reservoir characterization methodology and flow performance model for naturally fractured reservoirs.

The research has focused on estimating naturally fractured reservoir properties from seismic data, predicting fracture characteristics from well logs, and developing a naturally fractured reservoir simulator. It is important to develop techniques that can be applied to estimate the important parameters in predicting the performance of naturally fractured reservoirs. This project proposes a method to relate seismic properties to the elastic compliance and permeability of the reservoir based upon a sugar cube model. In addition, methods are presented to use conventional well logs to estimate localized fracture information for reservoir characterization purposes. The ability to estimate fracture information from conventional well logs is very important in older wells where data are often limited. Finally, a desktop naturally fractured reservoir simulator has been developed for the purpose of predicting the performance of these complex reservoirs. The simulator incorporates vertical and horizontal wellbore models, methods to handle matrix to fracture fluid transfer, and fracture permeability tensors.

This research project has developed methods to characterize and study the performance of naturally fractured reservoirs that integrate geoscience and engineering data. This is an important step in developing exploitation strategies for optimizing the recovery from naturally fractured reservoir systems. The next logical extension of this work is to apply the proposed methods to an actual field case study to provide information for verification and modification of the techniques and simulator.

This report provides the details of the proposed techniques and summarizes the activities undertaken during the course of this project. Technology transfer activities were highlighted by a two-day technical conference held in Oklahoma City in June 2002. This conference attracted over 90 participants and included the presentation of seventeen technical papers from researchers throughout the United States.

Table of Contents

Executive Summary and Introduction

Many existing oil and gas reservoirs in the United States are naturally fractured. It is estimated that from 70-90% of the original oil and gas in place in such complex reservoir systems are still available for recovery, provided new technology can be implemented to exploit these reservoirs in an efficient and cost effective manner. Enhanced oil recovery processes and horizontal drilling are two fundamental technologies which could be used to increase the recoverable reserves in these reservoirs by as much as 50%. This research is directed toward developing a systematic reservoir characterization methodology which can be used by the petroleum industry to implement infill drilling programs and/or enhanced oil recovery projects in naturally fractured reservoir systems in an environmentally safe and cost effective manner. This research program has been guided to provide geoscientists and engineers with techniques and procedures for characterizing a naturally fractured reservoir system and developing a desktop naturally fractured reservoir simulator, which can be used to select well locations and evaluate recovery processes to optimize the recovery of the oil and gas reserves from such complex reservoir systems.

The focus of the research is to integrate geoscience and engineering data to develop a consistent characterization of the naturally fractured reservoir. This report provides a summary of the activities conducted during this project in which techniques have been evaluated and developed for integrating the various data obtained in exploration and production activities to characterize the naturally fractured reservoir and predict the performance of these reservoirs.

Many of the factors controlling flow through naturally fractured reservoirs also dominate the seismic response of the reservoir. It is this relationship that offers the key to using seismic signals to predict important flow properties of naturally fractured reservoirs. These properties are important for reservoir characterization and numerical simulation of reservoir behavior. A sugar cube model has been developed for relating the elastic compliance and the permeability of fractured reservoirs. Using the sugar cube model to compute the dry or drained properties of fractured rocks, the results of Brown and Korringa (1975) have been utilized to derive expressions for predicting the compliances of fractured rocks as a function of saturation.

Results from the application and study of this approach to modeling indicate that Direct Hydrocarbon Indicators (DHI's) can be used for fractured reservoirs. This development opens a new window of exploration for fractured reservoirs. Surprisingly, this includes the application of S-waves for the detection of saturation changes in fractured reservoirs. In addition, a new laboratory/field approach to estimating connected porosity from permeability measurements is proposed. While neglecting the technical differences between flow and mechanical properties, the method offers a systematic approach to studying elastic and flow properties of naturally fractured reservoirs that requires further investigation. The sugar cube model can be used to integrate seismic studies in the assignment of important reservoir parameters for fractured reservoirs. As a result, both engineers and geophysicists end up discussing the same parameters controlling the performance of fractured reservoirs.

Characterization of naturally fractured reservoirs requires the integration of well, geologic, engineering and seismic data. Some of the data is available on a reservoir scale, such as the seismic data, while other data are available at the macroscale, such as well log data. A method is proposed for estimating well-based fractures parameters from conventional well log data. The ultimate use of this information is to take localized fracture information and scale it for

use in characterizing a naturally fractured reservoir and provide input parameters for reservoir simulation studies.

This research presents an approach to estimate the presence of fractures using conventional well logs using a Fuzzy Inference System. As all well logs are affected in some way by fractures, the Fuzzy Inference System is used to obtain a fracture index from the well log responses. The first step in determining the fracture characteristics from conventional well logs is to estimate the formation lithology. This can be done using several conventional techniques described in Bassiouni (1994) or Martinez, et al (2001). The techniques used depend on the logs available. Once the lithology of the formation has been determined, P- and S-wave velocities must be determined. The P-wave velocities can be obtained from the sonic logs, but S-wave velocities are rarely recorded. Several empirical models are available to estimate S-wave velocities from P-wave velocities (Xu and White, 1996 and Goldberg and Gurevich, 1998). The P- and S-wave velocities obtained can then be used to obtain fracture density and fracture aspect ratio from the inversion of a model from O'Connell and Budiansky (O'Connell, 1984).

Modifications to a generalized naturally fractured reservoir simulator developed by Ohen and Evans (1990) serve as the basis for the naturally fractured reservoir simulator. The simulator is a three-dimensional, three-phase black oil simulator developed to describe fluid flow in a naturally fractured reservoir based on the BOAST formulation. The simulator has the ability to model both vertical and horizontal wells. Flow into the wellbore from both the fractures and matrix is allowed to occur and is considered through productivity indexes that are proportional to the equivalent fracture and matrix permeabilities, respectively. For the horizontal well case, a wellbore system is implemented that assumes a horizontal well open to flow along its total length. The horizontal well model incorporates wellbore hydraulics.

In developing the fractured reservoir simulator, the BOAST-VHS code was translated from FORTRAN to Visual Basic and implemented with macros in an Excel-VB environment. This translation was undertaken to assist in providing a PC-based simulator that can be easily implemented without a major investment in computer hardware or software. The simulator was modified to incorporate Evan's naturally fractured reservoir model, the fracture permeability tensor, and the developed wellbore models. The resulting simulator was named BOAST-NFR to reflect the original source code and the NFR representing naturally fractured reservoir.

This research project has developed methods to characterize and study the performance of naturally fractured reservoirs that integrate geoscience and engineering data. This is an important step in developing exploitation strategies for optimizing the recovery from naturally fractured reservoir systems. The next logical extension of this work is to apply the proposed methods to an actual field case study to provide information for verification and modification of the techniques and simulator.

Results and Discussion

For many years, geoscientists and engineers have undertaken research to characterize naturally fractured reservoirs. Geoscientists have focused on understanding the process of fracturing and the subsequent measurement and description of fracture characteristics. Engineers have concentrated on the fluid flow behavior in the fracture-porous media system and the development of models to predict the hydrocarbon production from these complex systems. This research attempts to integrate these two complementary views to develop a quantitative reservoir characterization methodology and flow performance model for naturally fractured reservoirs.

This research has focused on estimating naturally fractured reservoir properties from seismic data, predicting fracture characteristics from well logs, and developing a naturally fractured reservoir simulator. It is important to develop techniques that can be applied to estimate the important parameters in predicting the performance of naturally fractured reservoirs. This project proposes a method to relate seismic properties to the elastic compliance and permeability of the reservoir based upon a sugar cube model. In addition, methods are presented to use conventional well logs to estimate localized fracture information for reservoir characterization purposes. The ability to estimate fracture information from conventional well logs is very important in older wells where data are often limited. Finally, a desktop naturally fractured reservoir simulator has been developed for the purpose of predicting the performance of these complex reservoirs. The simulator incorporates vertical and horizontal wellbore models, methods to handle matrix to fracture fluid transfer, and fracture permeability tensors.

Technology transfer activities were highlighted by a two-day technical conference held in Oklahoma City in June 2002. This conference attracted over 90 participants and included the presentation of seventeen technical papers from researchers throughout the United States.

This report provides the details of these techniques and summarizes the activities undertaken during the course of this project.

Task I. Characterize Fractured Reservoir Systems

When multiple fracture sets are present, both the permeability and the seismic response of fractured reservoirs can be more difficult to interpret. For example, the azimuthal variation of P-wave AVO may be quite strong over a single parallel set of fractures but considerably weakened when multiple fracture sets are present. An approach to the complexity of multiple fracture sets has been developed for modeling both the permeability and the compliance of fractured reservoirs in terms of an orthogonal set of fractures referred to as a sugar cube (Brown et al., 2002a).

The sugar cube model has been developed for relating the elastic compliance and the permeability of fractured reservoirs. Using the sugar cube model to compute the dry or drained properties of fractured rocks, the results of Brown and Korringa (1975) have been utilized to derive expressions for predicting the compliances of fractured rocks as a function of saturation.

Important results from the application and study of this approach to modeling includes the following:

1. Contrary to years of popular misconception, Direct Hydrocarbon Indicators (DHI's) can be used for fractured reservoirs. This development opens a new window of exploration for fractured reservoirs. Surprisingly, this includes the application of S-waves for the detection of saturation changes in fractured reservoirs.

2. A new laboratory/field approach to the study of reservoir rocks is suggested in terms of the sugar cube model. The basic idea is to assume that permeability measurements give a representation of the connected fracture porosity within a rock. The connected porosity determined by permeability measurements is assumed to also control the elastic anisotropy due to the fractures. These ideas neglect some of the technical differences between flow and mechanical properties but offer a systematic approach to the study of elastic and flow properties.
3. The sugar cube model can be used to integrate seismic studies in the assignment of important reservoir parameters for fractured reservoirs. As a result, both engineers and geophysicists end up discussing the same parameters controlling the performance of fractured reservoirs.

This section provides a brief description of how fracture permeability and compliance can be modeled using the sugar cube. Next arguments are given for uniting the permeability and compliance models in terms of an integrated mechanical and flow model of fractured reservoirs. The elastic compliance part of the model is used to explain how both P- and S-waves can be used to detect hydrocarbons directly in fractured reservoirs. This result is very important to future exploration efforts for fractured reservoirs. In addition to this useful result for exploration, methods of calibrating important reservoir and seismic parameters associated with the model will be discussed.

Permeability via the Sugar Cube Model

Both the permeability and the elastic compliance for a fractured reservoir can be expressed in terms of three orthogonal fracture sets. This is an important concept because it simplifies the approach to analyzing data over reservoirs that may or may not have multiple fracture systems. For example, there is no need to estimate the angles between the respective fracture sets that may exist since the same results can be obtained via the sugar cube model.

The permeability tensor for a single set of parallel fractures can be written in the form

$$k_{ij}^{f} = \frac{\left(\phi^{f}\right)_1}{12} A^2 \left(\delta_{ij} - n^{f}{}_{i} n^{f}{}_{j}\right) \quad \text{.....1}$$

where $(\phi^f)_1$ is the crack or fracture porosity and the subscript 1 indicates that this represents the porosity for a fracture set with a normal (n_i) in the x_1 direction. The aperture A represents the dimension of the opening in the crack through which the flow takes place. Figure 1 illustrates the permeability matrix for this model. Note that the x_1 component of permeability is zero. There is no flow perpendicular to a singular fracture set when the matrix or background is assumed to have no permeability.

Oda (1985) suggests that the resulting permeability for multiple fracture sets with normals in different directions can be computed by simply adding the permeabilities of individual sets (Eq. 1).

$$k_{ij}^{f} = k_{ij}^{1} + k_{ij}^{2} + k_{ij}^{3} + \ldots \quad \text{.....2}$$

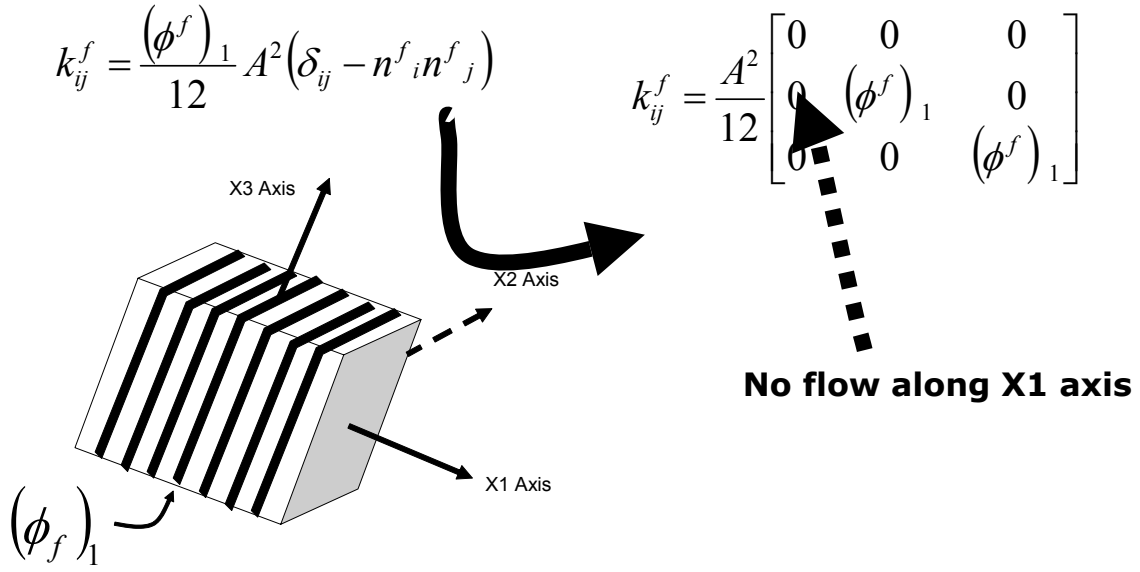

Fig. 1. Illustration of a single fracture set with normals in the direction of the X1 axis. This set will represent the largest fracture set (the set with the most porosity) in the sugar cube fracture model.

In this case the permeability matrix can be written in the form

$$k_{ij}^f = \begin{bmatrix} k_{11}^f & k_{12}^f & k_{13}^f \\ k_{21}^f & k_{22}^f & k_{23}^f \\ k_{31}^f & k_{32}^f & k_{33}^f \end{bmatrix} \quad \text{.....3}$$

where each of the terms in the matrix represent the sums of the fracture sets represented by Eq. 1.

In spite of the years of research applied to the study of fractured reservoirs, there is still a great deal that is not known at this time about the relationship between crack geometry and permeability. For example, even if a geologist or geophysicist could potentially identify and point out every fracture in a rock, there is no unanimous understanding of how to predict the fluid flow through that rock. This is not a small gap in our understanding! Oda (1985) and Brown and Bruhn (1998) attempted to correct for this lack of knowledge using a correction factor applied to Eq. 3. For example, Eq. 3 could be written in the form

$$k_{ij}^f = \lambda \begin{bmatrix} k_{11}^f & k_{12}^f & k_{13}^f \\ k_{21}^f & k_{22}^f & k_{23}^f \\ k_{31}^f & k_{32}^f & k_{33}^f \end{bmatrix} \quad \text{.....4}$$

where λ represents a correction factor for the physical problems neglected by simply adding the results of individual fractures or fracture sets. Problems such as the connectivity and roughness of the fractures can potentially be taken into account using this approach to fracture permeability.

This approach is seen as an attempt to match a detailed mechanical understanding, i.e., the exact locations of the fractures, to some type of understanding of the flow through the system. This type of approach is indeed necessary when attempting to make an estimate of the permeability based upon field observations. However, this approach is not recommended for an exploration environment. The problem is that of getting universal agreement upon a description of the pore space and the resulting permeability of that pore space. In other words, there is no easy measurement available for characterizing the permeable pore space.

As an alternative to the conventional thinking described above where the mechanical and flow views of the rock are distinct, it is suggested that the mechanical and flow modeling be integrated in the same model. This can be accomplished by deciding ahead of time that one way to study the fracture geometry that controls flow through a rock is via the measurement of the fracture permeability tensor for a rock. Assuming the permeability measurements have been carefully made, most people will agree that some indication of the porosity controlling the flow can be gained from this data. Getting agreement upon a measurement of fracture geometry and its meaning is a major accomplishment in the study of fractures.

In order to implement this approach to characterizing the fracture pore spacing controlling flow, it is suggested is that Eq. 1 be used exactly as it stands without the correction factor in Eq. 4. In essence this means that the fracture porosity and the fracture apertures will not be correct in an absolute sense. In a field environment there is no easy way to verify either of these variables directly. Thus we are giving up absolute values of the fracture porosity and aperture. What we are really after is the ability to predict the flow process through fractured reservoirs. In other words, we need to have the correct product of the aperture squared times the fracture porosity that will yield the measured permeability.

Now presume that Eq. 3 represents the measured fracture permeability in the measurement coordinate system. It is always possible to find a coordinate system in which this matrix can be expressed in a diagonalized form.

$$k_{ij}^{f} = \begin{bmatrix} k_{11}^{f} & 0 & 0 \\ 0 & k_{22}^{f} & 0 \\ 0 & 0 & k_{33}^{f} \end{bmatrix} \quad \text{.....5}$$

This matrix can be written using Eq. 1 in the form

$$k_{ij}^{f} = \frac{A^2}{12} \begin{bmatrix} (\phi_f)_2 + (\phi_f)_3 & 0 & 0 \\ 0 & (\phi_f)_1 + (\phi_f)_3 & 0 \\ 0 & 0 & (\phi_f)_1 + (\phi_f)_2 \end{bmatrix} \quad \text{.....6}$$

or

$$k_{ij}^{f} = \frac{A^2 \phi_f}{12} \begin{bmatrix} (\Delta\phi_f)_2 + (\Delta\phi_f)_3 & 0 & 0 \\ 0 & (\Delta\phi_f)_1 + (\Delta\phi_f)_3 & 0 \\ 0 & 0 & (\Delta\phi_f)_1 + (\Delta\phi_f)_2 \end{bmatrix} \quad \text{.....7}$$

of three orthogonal fracture sets with normals pointed along the principal axes of the fracture permeability tensor. The term in front of the matrix will be referred to as the scalar permeability factor, k_{SCF}.

$$k_{SPF} = \frac{A^2 \phi_f}{12} \quad \text{.....8}$$

This factor is important because it represents the measurement of a well test. Once again the subscripts on the porosities represent the directions of the normals for the fracture sets represented. The fractional or relative permeabilities of the orthogonal fracture sets in the sugar cube represent the individual fracture porosity divided by the total fracture porosity of the sugar cube (the sum of the fracture porosities for the three fracture sets).

$$(\Delta\phi_f)_i = \frac{(\phi_f)_i}{\phi_f} \quad \text{.....9}$$

The assumption is made in Eqs. 6 and 7 that the aperture is the same for all the fracture sets. In other words, the porosity is assumed to be the controlling factor upon the directional property of the permeability and Eq. 7 is used to assign the porosities to the orthogonal fracture sets when the eigenvalues of the fracture permeability, i.e., the diagonal values in Eq. 5, are known from measurements. This sugar cube model representing three orthogonal fracture sets is illustrated in Figure 2.

If the permeability eigenvalues are placed in the ascending order as shown below (S=smallest, I=Intermediate, L=Largest)

$$k_{ij}^{f} = \begin{bmatrix} K_S & 0 & 0 \\ 0 & K_I & 0 \\ 0 & 0 & K_L \end{bmatrix} \quad \text{.....10}$$

we can use the above measurement results to estimate the relative porosities of the sugar cube. When permeability is measured, both the background and the fracture permeability are determined. Assume that the three background values in the principal coordinate system of the fractures are KSB, KIB and KLB. Then the following three equations can be set up to determine the relative porosities for the sugar cube model.

$$KS = KSB + k_{SPF}\left[(\Delta\phi_f)_2 + (\Delta\phi_f)_3\right] \quad \text{.....11a}$$

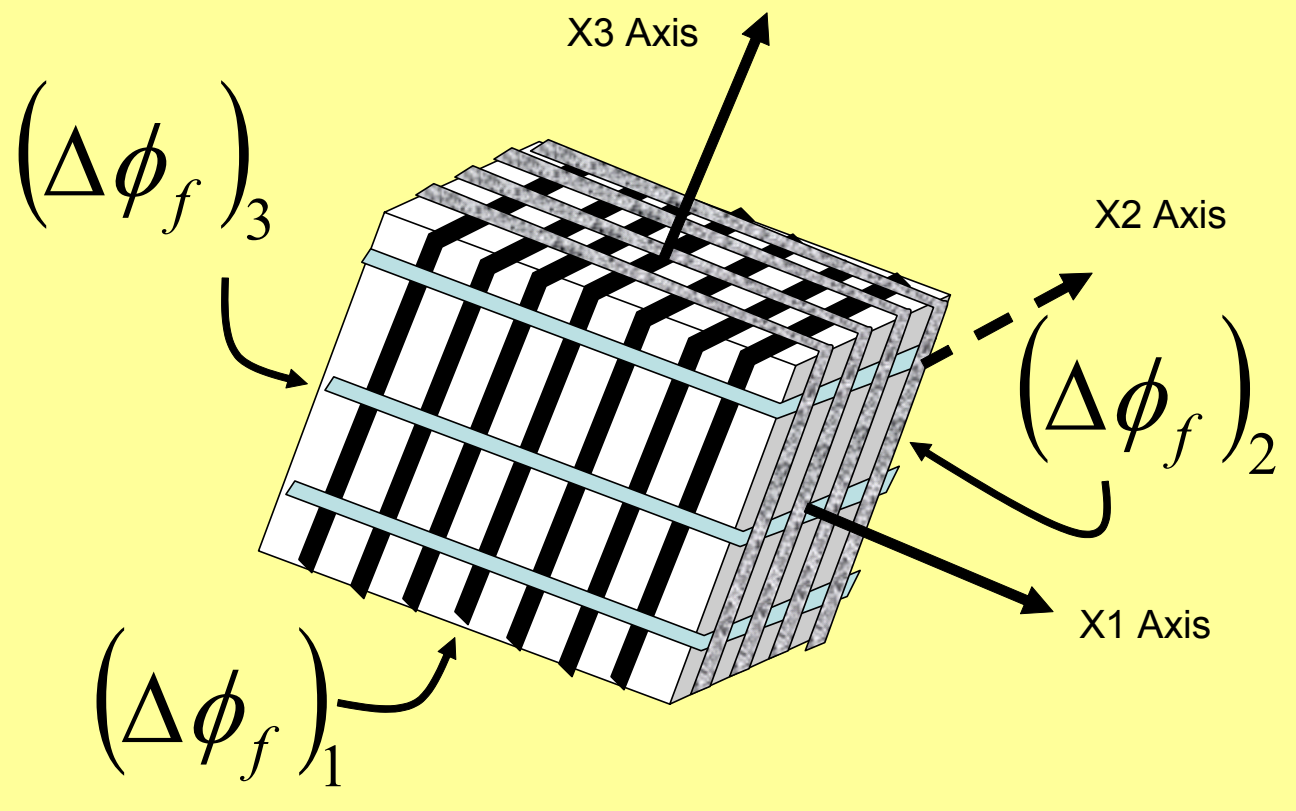

Fig. 2. Schematic illustration of the sugar cube model. The chosen convention will be to always have the most porous fracture set with normals along the x_1 axis, the set with intermediate porosity with normals pointed along the x_2 axis and the least porous set of fractures with normals along the x_3 axis.

$$KI = KIB + k_{SPF}\left[(\Delta\phi_f)_1 + \Delta\phi_f)_3\right] \quad \text{.....11b}$$

$$KL = KLB + k_{SPF}\left[(\Delta\phi_f)_1 + (\Delta\phi_f)_2\right] \quad \text{.....11c}$$

The scalar permeability factor is found by adding the three equations and using the fact that the sum of the relative porosities is equal to one.

$$k_{SPF} = \frac{(KL - KLB) + (KI - KIB) + (KS - KSB)}{2} \quad \text{.....12}$$

Once the scalar permeability factor is found, Eqs. 11a-c can be used to find the relative porosities for the sugar cube model. These relative porosities represent the characterization of the pore space controlling the fracture permeability. This idea for characterizing the fracture permeability has been illustrated by Brown et al. (2002a) using laboratory measurements of the permeability tensor made by Rasolofosaon and Zinszer (2002).

In summary, the directional controls for fracture permeability are assumed to be the relative porosities for the fracture sets involved. These directional features are quantified by the relative porosities of the sugar cube and they can be determined from the permeability. The convention of orienting the sugar cube so that the fracture sets with the largest, intermediate and smallest permeabilities have their normals pointed along the x_1, x_2 and x_3 axes respectively. The reason for the convention is to force agreement with the principal coordinate system for the compliance of the sugar cube discussed in the next section.

Elastic Compliance for the Sugar Cube Model

An approach similar to that used for the permeability can also be used for estimating the elastic compliance of a fractured rock (Schoenberg and Sayers, 1995).

$$S^f_{ijkl} = \frac{1}{4}\left(\begin{array}{l} \delta_{ik}\left[\sum_m Z^{(m)} n_l^{(m)} n_j^{(m)}\right] + \delta_{jk}\left[\sum_m Z^{(m)} n_l^{(m)} n_i^{(m)}\right] + \delta_{il}\left[\sum_m Z^{(m)} n_k^{(m)} n_j^{(m)}\right] \\ + \delta_{jl}\left[\sum_m Z^{(m)} n_k^{(m)} n_i^{(m)}\right] \end{array} \right) \quad \text{.....13}$$

where the summation notation again represents the sum of fracture sets with different normals. The quantities inside of the brackets represent the Kachanov matrix

$$\alpha_{ij} = \sum_m Z^{(m)} n_i^{(m)} n_j^{(m)} \quad \text{.....14}$$

As with the permeability tensor, there is a coordinate system in which the Kachanov tensor is diagonalized.

$$\alpha_{ij} = \begin{pmatrix} \alpha_1 & 0 & 0 \\ 0 & \alpha_2 & 0 \\ 0 & 0 & \alpha_3 \end{pmatrix} \quad \text{.....15}$$

where $\alpha_1 \geq \alpha_2 \geq \alpha$.

In the principal coordinate system of the Kachanov matrix, the compliance for multiple fracture sets can be written in the form

$$\underline{S}_f = \begin{bmatrix} \alpha_1 & 0 & 0 & 0 & 0 & 0 \\ 0 & \alpha_2 & 0 & 0 & 0 & 0 \\ 0 & 0 & \alpha_3 & 0 & 0 & 0 \\ 0 & 0 & 0 & \alpha_2+\alpha_3 & 0 & 0 \\ 0 & 0 & 0 & 0 & \alpha_1+\alpha_3 & 0 \\ 0 & 0 & 0 & 0 & 0 & \alpha_1+\alpha_3 \end{bmatrix} \quad \text{.....16}$$

Brown et al. (2002 a, 2002b) have illustrated how Eq. 16 can be written in the form

$$\underline{\underline{S}}_f = Z_{SCF}\begin{bmatrix} (\Delta\phi_C)_1 & 0 & 0 & 0 & 0 & 0 \\ 0 & (\Delta\phi_C)_2 & 0 & 0 & 0 & 0 \\ 0 & 0 & (\Delta\phi_C)_3 & 0 & 0 & 0 \\ 0 & 0 & 0 & (\Delta\phi_C)_2+(\Delta\phi_C)_3 & 0 & 0 \\ 0 & 0 & 0 & 0 & (\Delta\phi_C)_1+(\Delta\phi_C)_3 & 0 \\ 0 & 0 & 0 & 0 & 0 & (\Delta\phi_C)_1+(\Delta\phi_C)_3 \end{bmatrix} \quad \text{.....17}$$

where once again the relative porosities of a sugar cube model control the anisotropy of the fractures. The scalar compliance factor (Z_{SCF}) is the product of the fracture porosity and a factor referred to here as the weakness (W).

$$Z_{SCF} = W\phi_f \quad \text{.....18}$$

Now the background compliance has to be added in order to obtain the total compliance of the rock.

Unifying the Models

The assumption is made that the sugar cube porosity distribution representing the flow through the fractures is the same sugar cube representing the compliance of the fractures. This is not a correct assumption in an absolute sense but it has the practical advantage of giving a direct relationship between seismic and flow measurements. This means that we can make measurements of the permeability tensor to assign properties to the cracks through which flow takes place. Then we can use that model for the fractures gained from permeability measurements to predict the seismic response for the fractures controlling flow through the rock. The advantage of this model is that both permeability and seismic measurements can be integrated into an interpretation of the rock properties. As a result, the mixed mechanical and flow modeling gives a new direction and thinking for both laboratory and field measurements.

Understanding the Background

The challenge in using the sugar cube model is that it presumes that the background can be found. The combined effects of the background or matrix and the fractures control measurements made upon fractured rocks. Thus the background affects both the measured compliance and the permeability.

$$k_{ij}^{Measured} = k_{ij}^{BACKGROUND} + k_{ij}^{f} \quad \text{.....19}$$

$$S_{ijkl}^{Measured} = S_{ijkl}^{BACKGROUND} + S_{ijkl}^{f} \quad \text{.....20}$$

If we are lucky, the background will be homogeneous. For the permeability, the matrix or background permeability may often be close to zero for many rocks so that the permeability measurement is a direct measure of the properties of the sugar cube representing the fractures.

The background compliance can be quite complicated. For example, there may be open or closed cracks that do not participate in the flow. Estimating the background compliance is an important aspect of using seismic signals to predict the flow through the fractures in a rock.

Brown et al. (2002a) have used the permeability and compliance measurements of Rasolofosaon and Zinszer (2002) to examine fracture geometry via the permeability, the background compliance and the scalar compliance factor in Eq. 18. The basic idea used in that paper can be described by rewriting Eqs. 17 and 20 in the 6x6 form

$$S_{ij}^{Measured} = S_{ij}^{BACKGROUND} + S_{ij}^{f} \quad = \quad S_{ij}^{BACKGROUND} + Z_{SCF} R_{ij} \qquad \text{.....21}$$

where the R_{ij} matrix depends upon the relative porosities of the sugar cube. When these can be determined using permeability measurements as described above, the compliance of the fractures can be determined if the scalar compliance factor (Z_{SCF}) is known. In this case a direct estimate of the background properties for a rock is possible.

$$S_{ij}^{BACKGROUND} = \quad S_{ij}^{Measured} - Z_{SCF} R_{ij} \qquad \text{.....22}$$

In general the scalar compliance factor will not be known and a value consistent with the expected properties of the background will have to be used (Brown et al., 2002a). This is one approach to calibrating the scalar compliance factor and/or the weakness factor in Eq. 18.

In summary, a unified flow and mechanical model ignores a great deal of the physics involved but offers a systematic approach to integrating seismic and flow measurements in both the laboratory and the field. The challenge to using this approach to modeling fractured reservoirs is the separation of the effects of the background from those of the fractures. The sugar cube model lays the foundation for relating background to fracture properties.

Predicting the Effects of Saturation upon Fractured Reservoirs

A popular misconception within the industry is that saturation effects cannot be detected using seismic signals in fractured reservoirs. This misconception has occurred because of predictions based upon the classic Gassmann (1951) equation which predicts the effects of fluid saturation upon the elastic properties of isotropic rocks. The basic thinking appears to be that the hard rocks that are fractured are so hard that any fluid can be placed into the pore space and the effects will not be noticed. The problem with this thinking is that it ignores the softening of the rock due to the presence of the fractures. A more technical explanation can be given in terms of the results of Brown and Korringa (1975).

$$S_{ijkl}^{*} = S_{ijkl}^{A} - \frac{\left(S_{ij}^{A} - S_{ij}^{M}\right)\left(S_{kl}^{A} - S_{kl}^{M}\right)}{\left[\left(K_{FLUID} - K_{\phi}\right)\phi + \left(K_{A} - K_{M}\right)\right]} \qquad \text{.....23}$$

Here the superscript * represents the effective compliance of a fractured rock filled with a saturating fluid. The superscript A represents the dry (fractured) rock. The superscript M represents the background. The K's represent scalar (or isotropic) compliances. Subscripts A and M for the scalar compliances represent the dry rock and background scalar compliances. The scalar compliance with the subscript FLUID represents the compliance of the saturating fluid.

The scalar compliance with the subscript ϕ represents the pore space compliance. If the fracture porosity controls the difference between the dry rock and the background rock (superscript M), then we can write

$$S_{ij}^{A} = S_{ij}^{M} + S_{ij}^{f} \quad \text{.....24}$$

Then neglecting the pore space compliance since it should have a value close to that of the background (superscript M), Eq. 23 can be written in the form

$$S_{ijkl}^{*} = S_{ijkl}^{M} + S_{ijkl}^{fracture} - \frac{\left(S_{ij}^{fracture}\right)\left(S_{kl}^{fracture}\right)}{\left[\left(K_{FLUID} - K_{\phi}\right)\phi + \left(K_{fracture}\right)\right]} \quad \text{.....25}$$

The first two terms on the right hand side of Eq. 25 represent the dry rock compliance and the last term represents the influence of a saturating fluid upon the compliance of the fractured rock. If the fracture compliances are written in terms of the sugar cube model, the following equation can be used to describe the compliance of a saturated reservoir rock (Brown et al., 2002d).

$$S_{ij}^{*} = S_{ij}^{M} + Z_{SCF} R_{ij} - \frac{\left(Z_{SCF}\right)^{2}}{K_{FLUID}\phi_{f} + Z_{SCF}} T_{ij} \quad \text{.....26}$$

where the R and T matrices are written in terms of the relative porosities of the sugar cube model. Eq. 26 can be used to predict the effects of saturation upon fractured reservoirs. The first two terms represent the fractured dry rock while the last term represents the effect of the fluid saturation. If the scalar compliance factor is small compared to the product of the fluid compliance and the fracture porosity, the effects of saturation are negligible. When the scalar compliance factor is large enough, the effect of saturation becomes important.

Based upon an extensive study of a field in Oman by Shell (Guest et al., 1998) the effects of saturation can indeed be observed using seismic data. In the Shell study, S-wave splitting was observed to increase when going from the brine saturated to the gas saturated portion of the reservoir (Fig. 3). Brown et al. (2002c, 2002d, 2002e) have interpreted these results in terms of the tilt of the fractures away from the vertical. Thus both P- and S-waves can show the effects of saturation in fractured reservoirs.

In order to explain the Shell observations, we can use an approximate approach by writing the compliance terms from Eq. 26 that most affect vertically traveling S-waves.

$$S_{44} = S_{44}^{M} + Z_{SCF}(\beta_{22} + \beta_{33}) - \left(\frac{\left(Z_{SCF}\right)^{2}}{K_{FLUID}\phi_{f} + Z_{SCF}}\right) 16(\beta_{23})^{2} \quad \text{.....27a}$$

$$S_{55} = S_{55}^{M} + Z_{SCF}(\beta_{11} + \beta_{33}) - \left(\frac{\left(Z_{SCF}\right)^{2}}{K_{FLUID}\phi_{f} + Z_{SCF}}\right) 16(\beta_{13})^{2} \quad \text{.....27b}$$

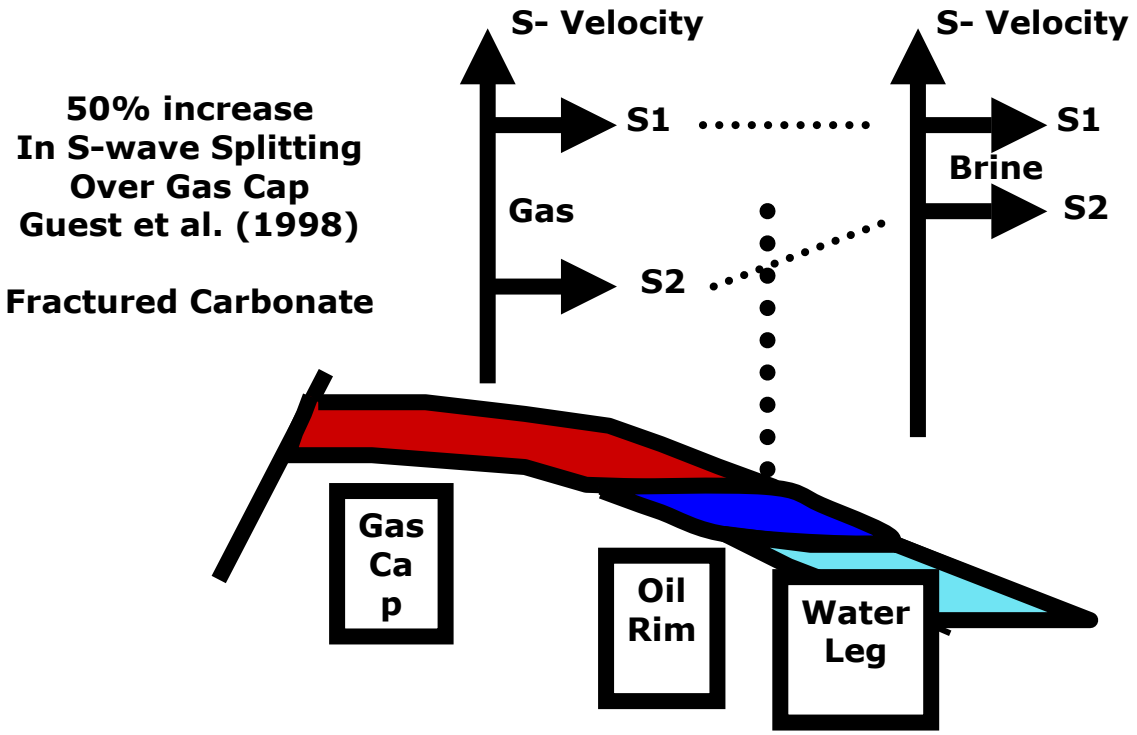

Fig. 3. A Shell study indicated that the S-wave splitting over a fractured carbonate reservoir increased by 50% when going from the brine-saturated to the gas-saturated portion of the reservoir.

The S_{44} is an approximation to the compliance affecting the fastest S-waves while the S_{55} term is an approximation to the compliance of the slow S-wave. In practice the phase and group velocity are computed, but Eq. 26 can be used to give an intuitive discussion of what happens to S-waves when a fractured reservoir is saturated.

If the sugar cube model is vertically aligned ($\beta_{13} = \beta_{23} = 0$), the two saturation terms on the right in Eq. 27 are zero. In this case, there is no stiffening of the fractures due to saturation and the S-wave splitting is a function of the differences in porosity between the fracture sets in the sugar cube. However, when the sugar cube is tilted, the effects of saturation become important and the S-wave splitting can be modified. The modification depends upon the direction in which the sugar cube is tilted. Fig. 4 illustrates the effect upon S-wave splitting when the major fracture set in the sugar cube is tilted away from the vertical ($\beta_{13} \neq 0$). This is exactly the effect observed during the Shell study.

Now when the sugar cube is tilted so that the intermediate fracture set in the sugar cube is tilted away from the normal ($\beta_{23} \neq 0$), then the S-wave splitting increases when going from gas to brine. This is just the opposite of what took place when the largest fractures were tilted away from the vertical. Fig. 5 illustrates the S-wave splitting for this case. Thus the direction of the S-wave splitting is not an indication of the gas in the reservoir unless the dip of the fractures is understood.

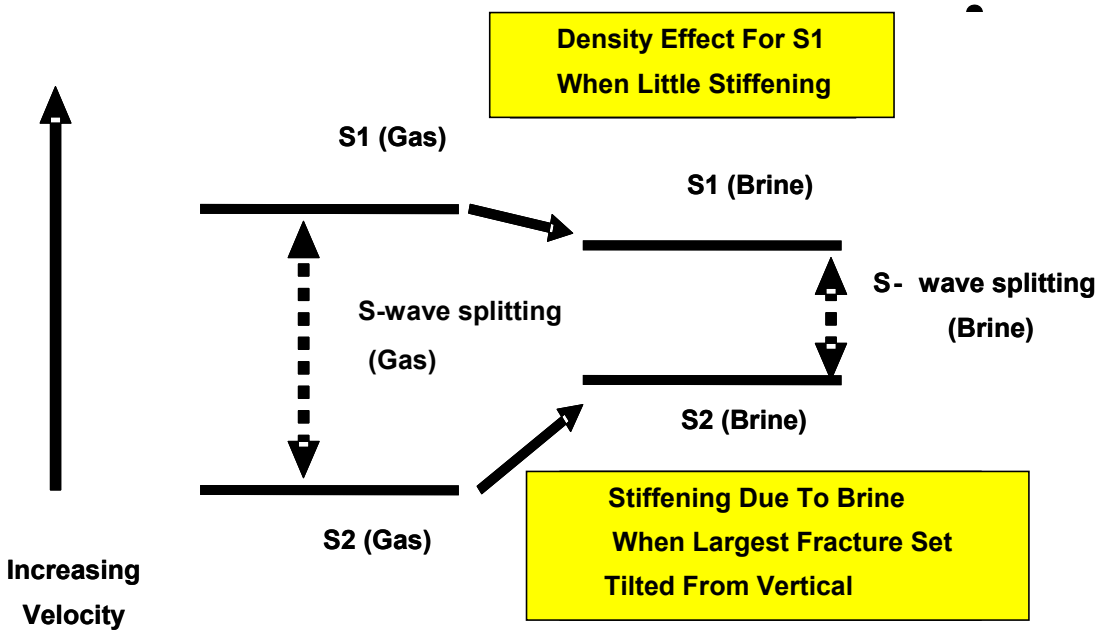

Fig. 4. Figure illustrating how the S-wave splitting is affected when saturation changes and the sugar cube is tilted toward the normal of the largest fracture set. This is the effect observed by the Shell study at Oman.

The important point made by the Shell study is that fractures can soften even the hardest rocks to the point where the effects of saturation can be observed. The problem is that for P-wave recording from the surface, long offsets between source and receiver are required. S-waves do not require long offsets but offer other problems. However, the problems facing both of these issues should be overcome now that there is a motivation in terms of the exploration for fractured reservoirs.

One valuable aspect of saturation changes in a reservoir is the chance to calibrate the scalar compliance factor. For example, the Shell observations indicated that the S-wave splitting increased by 50%. If we write the S-wave splitting in the form

$$\Delta = \frac{V_1 - V_2}{V_1} \frac{\sqrt{\frac{1}{S_{44}\rho}} - \sqrt{\frac{1}{S_{55}\rho}}}{\sqrt{\frac{1}{S_{44}\rho}}} \quad \text{.....28}$$

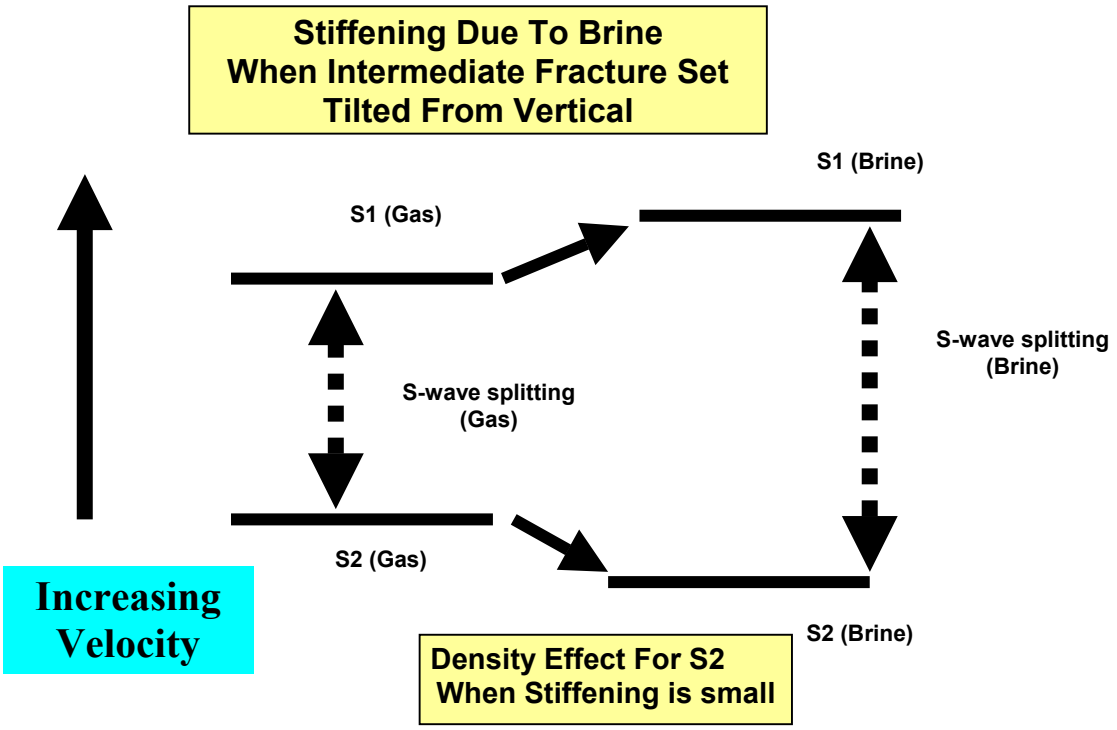

Fig. 5. Schematic illustrating how the S-wave splitting is affected when saturation changes and the sugar cube is tilted toward the normal of the intermediate fracture set in the sugar cube.

Using an isotropic background (carbonate with an S-wave velocity of 8500 f/s, 2591 m/s) and a sugar cube with the following relative porosities ($(\Delta\phi)_1 = .6,\ (\Delta\phi)_2 = .3,\ (\Delta\phi)_3 = .1$) the S-wave splitting in the brine will be 7% and S-wave splitting in the gas will be 11% (a 50% increase) when the major fracture set is tilted 10 degrees away from the vertical. The scalar compliance used for this computation was $Z_{SCF}=1x10^{-10}$ (1/Pa) and the porosity is assumed to be 2%. In other words, saturation changes give valuable calibration information for the elastic properties of fractured rocks and help to quantify the relative magnitudes of the fracture porosity and the fracture weakness (W) for the scalar compliance factor in Eq. 18.

In summary, saturation changes in fractured reservoirs offer valuable information for both exploration and development. Both P- and S-wave data can be used but each offers special problems in order to observe the effects of saturation. When saturation effects can be observed, the results can be used to calibrate the seismic response.

Integration of Seismic and Production Data - Fractured Reservoirs

One of the main reasons for moving to the integrated sugar cube model suggested here is the ability to integrate production and seismic data. Seismic data gives a measure of the fracture compliance which is weighted by a scalar compliance factor. If we have a good idea of the background compliance then we can estimate the scalar compliance factor.

$$Z_{SCF} = W\phi_f \quad \text{.....29}$$

However, this is a product and to really use the seismic away from the well control, we need to evaluate the weakness of the fractures (W) so the porosity can be predicted away from the well control. Unfortunately it is very difficult to estimate fracture porosity via well logs.

Production tests in fractured reservoirs offer one way to get fix the estimated fracture porosity at the well. There the scalar permeability factor is determined.

$$k_{SPF} = \frac{A^2\phi_f}{12} \quad \text{.....30}$$

as well as the spacing (L) for the fractures. Any number of engineering models might then be used to fix the fracture porosity so the value obtained is consistent with the well test. Assume for example that the porosity can be computed using the porosity for a single set of fractures in the form

$$\phi_f = \frac{A}{A+L} \quad \text{.....31}$$

Admittedly this deviates from the sugar cube model, but we are calibrating with a well test model that assumes only one parameter (L) for describing the size of the matrix blocks. After the spacing has been determined, the aperture is fixed to give the measured permeability at the well.

In summary, the well test data and saturation changes can be used to estimate the weakness of the fractures. Once this type of calibration is established the fracture porosity can be mapped throughout the field using seismic data. This seismic picture of the fracture porosity can be modified via the application of well tests that are used to estimate the spacing (L) and the apertures.

Summary

In summary, permeability and compliance models for multiple fracture systems have been merged assuming that they are represented by the same fracture porosity. Although this approach ignores some of the basic physical differences between flow properties and mechanical properties of fractures, it does offer a format through which the two distinct problems can be studied in tandem. Measurement of the fracture permeability tensor is a reliable indicator of the fracture geometry controlling flow when the background effects have been eliminated. The integrated sugar cube model introduced here is applicable for both laboratory and field studies. Both environments offer distinct advantages. For example, the laboratory environment can be used to determine the complete compliance tensor and the permeability tensor. However, it is more difficult in a laboratory environment to estimate the background properties because of the smaller samples. The field environment offers a reduced angular coverage making it more difficult to determine the relative porosities for the sugar cube model. However, because of the larger scale and the well tests, the background and key properties of the fracture/matrix system can be obtained.

We have applied the sugar cube model combined with the results of Brown and Korringa (1975) to illustrate how saturation can be detected in fractured reservoirs. The emphasis in this report was upon the fact that S-waves can be used to detect saturation. This is indeed a surprising result. There are those who might say the fact that S-waves may be sensitive to saturation has been known for a long time [e.g., since the publication of the paper by Brown and Korringa(1975)]. However, only recently with the field study by Shell (Guest et al., 1998) was it apparent that the saturation of fractures could indeed be detected by S-waves. That study clearly indicates that the fractures weakened the rock sufficiently to show effects upon both P- and S-waves. The problem with the P-waves is that they must be traveling at large angles (large offset) in order to be sensitive to the saturation of the fractures. Near-vertical S-waves can be used to detect the saturation changes as well. The choice between the two is a function of many variables including the cost.

The integrated sugar cube model has been applied to laboratory data in which both the compliance and permeability tensors were determined. Such a study can be used to calibrate important fracture properties at the laboratory scale. In the study of fractures using laboratory data (Brown et al., 2002a, 2002d, 2002e), the fractures were found to be too stiff in order to show the effects of saturation. The primary effects due to saturation changes found in that study were density changes without the stiffening effect (changes in the compliance). The Shell study indicates the antithesis of this result giving a clear picture of the stiffening effects due to saturation. This indicates a definite difference in the weakness of the fractures studied in the laboratory and those observed in the field by the Shell study.

Finally, methods for calibrating and integrating seismic and production data have been illustrated using the sugar cube model. When spacing and aperture can both be defined using well tests, the seismic measurements can be used to estimate fracture porosity throughout the reservoir. If the effective aperture is constant throughout the field, this means that the calibrated seismic can be used to estimate the fracture spacing as well as the permeability throughout the reservoir.

Task II. Develop Interwell Descriptors of Fractured Reservoir Systems

Characterization of naturally fractured reservoirs requires the integration of well, geologic, engineering and seismic data. Some of the data is available on a reservoir scale, such as the seismic data, while other data are available at the macroscale, such as well log data. In this task, the desire was to take localized fracture information and scale it for use in characterizing a naturally fractured reservoir and provide input parameters for reservoir simulation studies. Effort focused on estimating well-based fracture parameters from conventional well log data.

The first step in determining the fracture characteristics from conventional well logs is to estimate the formation lithology, including the clay content. This can be done using several conventional techniques described in the Bassiouni (1994) text and has been presented in Martinez, et al (2001). The technique to obtain the remaining lithology fractions depends on the logs available. These techniques also can be found in Bassiouni (1994) and Martinez, et al (2001).

Once the lithology of the formation has been determined, P- and S-wave velocities must be determined. The P-wave velocities can be obtained from the sonic logs, but S-wave velocities are rarely recorded. Several empirical models are available to estimate S-wave velocities from P-wave velocities (Xu and White, 1996 and Goldberg and Gurevich, 1998). The technique used in this work is from Greenberg and Castagna, 1992.

This model is a semi-physical model to predict shear wave velocity in porous rocks using the measured P-wave velocity. The authors assumed that all petrophysical parameters influence the compressional wave velocity in the same way as the shear wave velocity, and an empirical relationship between V_p and V_s in a porous brine-saturated medium was proposed.

For each pure lithology constituent, the relationship between V_s and V_p was given by:

$$V_s^{\text{pure}\,i} = a_{2i}V_p^2 + \cdots + a_{1i}V_p + a_{0i} \quad \text{.....32}$$

where, V_p is the P-wave velocity, a_{2i}, a_{1i} and a_{0i} are empirical coefficients for pure component i and $V_s^{pure\,i}$ is the shear wave velocity for pure component i.

The authors proposed the Voight–Reuss–Hill (VRH) average as a mixing rule to obtain the shear wave velocity for the given rock:

$$V_s = \frac{1}{2}\left[\left(\sum_{i=0}^{l} F_i V_s^{\,purei}\right) + \left(\sum_{i=0}^{l} \frac{F_i}{V_s^{\,purei}}\right)^{-1}\right] \quad \text{.....33}$$

where F_i is the volume fraction of pure component i. The lithology specific coefficients (with V_p and V_s in km/s) derived from core and log measurements are shown in Table 1. These coefficients are only valid for consolidated sedimentary rocks.

Table 1. Greenberg and Castagna's Lithology Specific Coefficients for V_p and V_s, km/s.

	$\mathbf{a_{2i}}$	$\mathbf{a_{1i}}$	$\mathbf{a_{0i}}$
Shale	0	0.76969	-0.86735
Sandstone	0	0.80416	-0.85588
Limestone	-0.05508	1.01677	-1.03049
Dolomite	0	0.58321	-0.07775

The P- and S-wave velocities obtained can then be used to obtain crack density and crack aspect ratio from the inversion of a model from O'Connell and Budiansky (O'Connell, 1984). Other comparable models of fractured rocks can be used for this purpose as well. The O'Connell and Budiansky model considers a solid permeated with two classes of porosity: crack-like, characterized by a crack density with fluid pressure equal to the applied normal stress on the crack face, and pore-like (i.e. tubes or spheres) characterized by a volume porosity, with fluid pressure substantially less than the applied hydrostatic stress. Fluid is allowed to flow between cracks at different orientations and between cracks and pores in response to pressure differences. With the propagation of a compressional wave, local pressure oscillations are expected to cause such fluid exchanges.

The model assumes elliptic cracks and spherical pores to estimate the strain of the composite rock. The parameters of this model are:

- The crack density, defined by:

$$\varepsilon = N * \frac{2}{\pi} \langle \frac{A^2}{P} \rangle \quad \text{.....34}$$

where N is the number of cracks per unit volume; A is the area in plain-form of the crack and P is the perimeter of the crack.

- The porosity of the spherical pores, ϕ.
- The fluid bulk modulus, K_f.
- The bulk and shear moduli of the uncracked non porous matrix material, K_o and G_o.
- Frequency, w.
- The characteristic frequency for fluid flow between cracks, w_s. This parameter can be estimated as:

$$w_s \approx 4\left(\frac{K}{\eta}\right)\left(\frac{c}{a}\right)^3 \quad \text{.....35}$$

where μ is the viscosity of the fluid, and c/a is the aspect (thickness to diameter) ratio of the crack.

The moduli are considered to be a function of frequency, w, and are complex quantities, the real part representing an effective elastic modulus, and the imaginary part representing anelastic energy dissipation.

The complex bulk modulus K is given by:

$$\frac{K}{K_o} = 1 - \frac{\left(1 - \frac{K_f}{K_o}\right)\left(\frac{3}{2}\left(\frac{1-v}{1-2v}\right)\phi + \frac{16}{9}\left(\frac{1-v^2}{1-2v}\right)\frac{\varepsilon}{1+i\Omega}\right)}{\left(1 + \frac{K_f}{2K}\left(\frac{1-v}{1-2v}\right)\right)\phi + \left(\frac{16}{9}\left(\frac{1-v^2}{1-2v}\right)\frac{K_f}{K}\frac{\varepsilon}{1+i\Omega}\right)}\phi \quad \text{.....36}$$

with:

$$\Omega = \frac{16}{9}\left(\frac{1-v^2}{1-2v}\right)\frac{K_o}{K}\frac{w}{w_s} \quad \text{.....37}$$

The shear modulus G is determined using:

$$\frac{G}{G_o} = 1 - \frac{15(1-v')}{7-5v'}\phi - \frac{32(1-v')}{45}\left(\frac{1}{1+i\Omega'} + \frac{3}{2-v'}\right)\varepsilon \quad \text{.....38}$$

$$\frac{K'}{K'_o} = 1 - \frac{3}{2'}\left(\frac{1-v'}{1-2v'}\right)\phi - \frac{16}{9}\left(\frac{1-v'^2}{1-2v'}\right)\left(\frac{\varepsilon}{1+i\Omega'}\right) \quad \text{.....39}$$

where v' is a fictitious Poisson ratio that satisfies:

$$v' = \frac{3K'-2G}{6K'+2G} \quad \text{.....40}$$

The same expression relates the moduli and Poisson ratio of the porous solid:

$$v = \frac{3K-2G}{6K+2G} \quad \text{.....41}$$

Since w_s can be approximated by Eq. 35, then the ratio w/w_s is given by:

$$\frac{w}{w_s} = \frac{w}{4\left(\frac{K}{\eta}\right)\left(\frac{c}{a}\right)^3} = \frac{Asp}{K} \quad \text{.....42}$$

where:

$$Asp = \frac{w\eta}{4\left(\frac{c}{a}\right)^3} \quad \text{.....43}$$

Then Eq. 37 can be rewritten as:

$$\Omega = \frac{16}{9}\left(\frac{1-v^2}{1-2v}\right)\frac{K_o}{K}\frac{Asp}{K} \quad \text{.....44}$$

and Ω' is given by:

$$\Omega' = \frac{16}{9}\left(\frac{1-v'^2}{1-2v'}\right)\frac{K_m}{K'}\frac{Asp}{K} \quad \text{.....45}$$

If shear and compressional wave velocities are given, then bulk and shear moduli can be directly obtained from the following equations:

$$K = \frac{\rho_b\left(V_P^2 - \frac{4}{3}V_S^2\right)}{10^6} \quad \text{.....46}$$

$$G = \frac{\rho_b \left(V_S^2\right)}{10^6} \quad \text{.....47}$$

where ρ_b is in g/cm^3, V_p and V_s are in m/s, and G and K in GPa.

Knowing K and G, Eqns. 36 – 39 can be solved simultaneously for crack density ε, and aspect ratio, c/a.

The general procedure to be applied in order to obtain crack density and aspect ratio is outlined by the following steps. These steps are summarized in the flow chart presented in Figure 6.

1. Gamma ray logs are used to obtain clay content.
2. The remaining lithology fractions are estimated using Pe, neutron porosity and density logs.
3. If the shear velocity log is not available, shear wave velocity at each depth is estimated using the Greenberg and Castagna model.
4. Fracture density and aspect ratio are obtained using the O'Connell and Budiansky inverse model presented above.

Additionally, Mavko, et al. (1998) have shown that once ε and α are known, crack porosity can be computed using:

$$\phi_c = \frac{4}{3}\pi\varepsilon\alpha \quad \text{.....48}$$

This equation will be used later to help determine potential zones of fracturing.

To test the model, a synthetic example was developed. Logs used include the caliper, Gamma Ray, Spontaneous Potential, Sonic, Neutron Porosity and Bulk Density logs. A Photoelectric log was also used as a lithology tool. Figure 7 shows the generated crack-density and aspect ratio logs.

Simultaneous solution for the inversion of the O'Connell and Budiansky model is an inefficient process. Thus, a more suitable technique to obtain crack density, ε, and aspect ratio c/a, was desired. The inversion of the O'Connell and Budiansky model can be seen as an optimization problem, where the goal is to minimize an objective function. If the real parts of the moduli moduli (K_r and G_r) are known, the inversion of the model consists of obtaining the parameters ε and c/a that will minimize an objective function given by:

$$F = \left|K_r - K_{rcal}\right| + \left|G_r - G_{rcal}\right| \quad \text{.....49}$$

where K_{rcal} and G_{rcal} are the real portions of the bulk and shear moduli obtained from the O'Connell and Budiansky model.

For this particular problem, conventional gradient optimization methods are not an appropriate method for obtaining a solution. Therefore a genetic algorithm approach was implemented and programmed using FORTRAN.

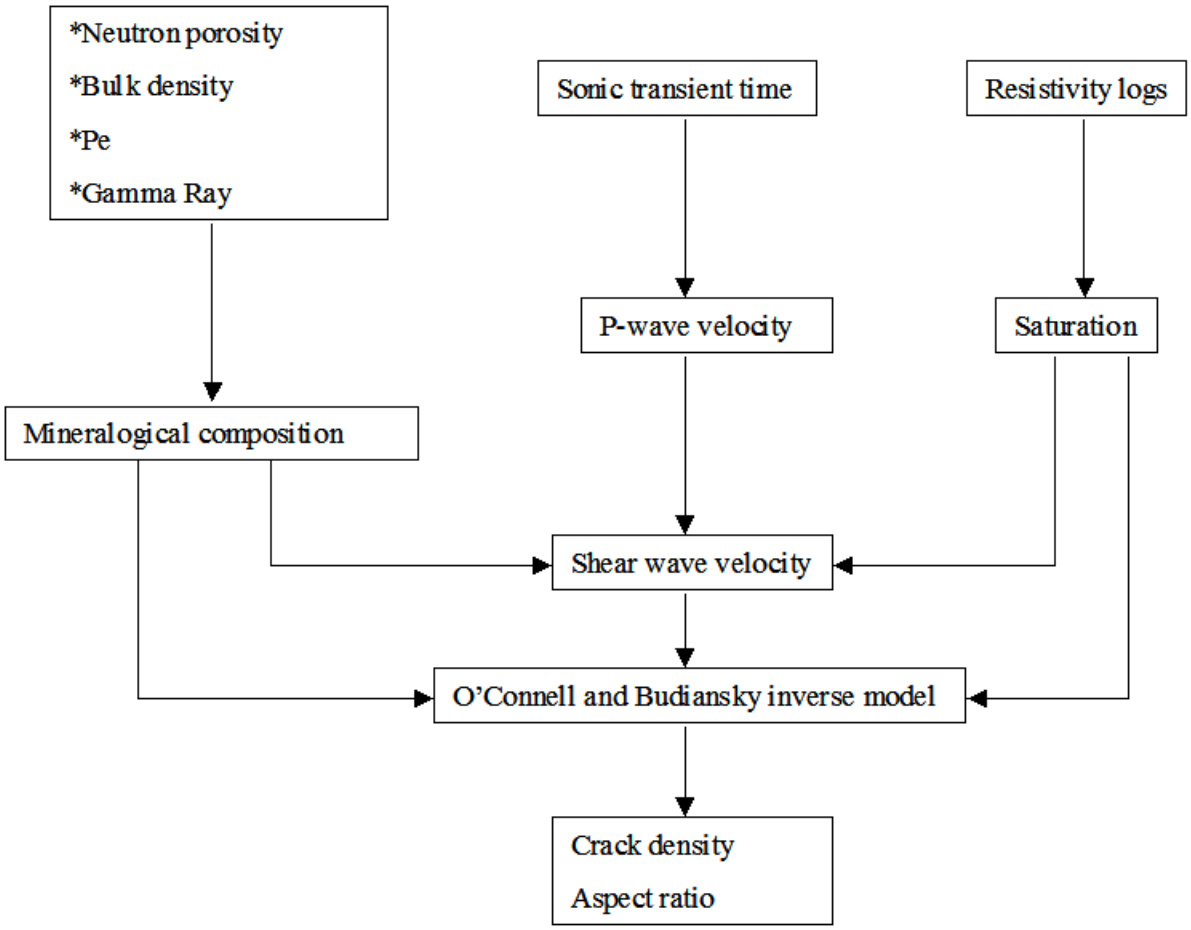

Fig. 6: Fracture Density And Aspect Ratio From Conventional Well Logs.

A 6×8 bit binary string formed the chromosomes, which represent the 6 unknown variables, K'_r, K'_c, K_c, G_c, α, ε, each with an eight-bit resolution. An initial population of 30 chromosomes was generated. Each chromosome was first randomly generated and then evaluated in order to guarantee that it was within the solution space. The randomly generated chromosome was decoded to obtain the generated values for K'_r, K'_c, K_c, G_c, α, and ε. Eqs. 40 and 41 were then used to verify that the Poisson's ratios were in the range between 0 and 1. If the chromosome satisfied these constraints, it was allowed into the population. Otherwise the chromosome was rejected and a new chromosome was randomly generated and evaluated until a population size of 30 chromosomes was obtained. Every chromosome within the population was evaluated using Eqs. 36, 38 and 39 with the real portions of the bulk and shear moduli as "output" parameters (K_{rcal} and G_{rcal}). The K_r and G_r terms are either obtained experimentally or can be computed when the compressional and shear wave velocities and the bulk density are known.

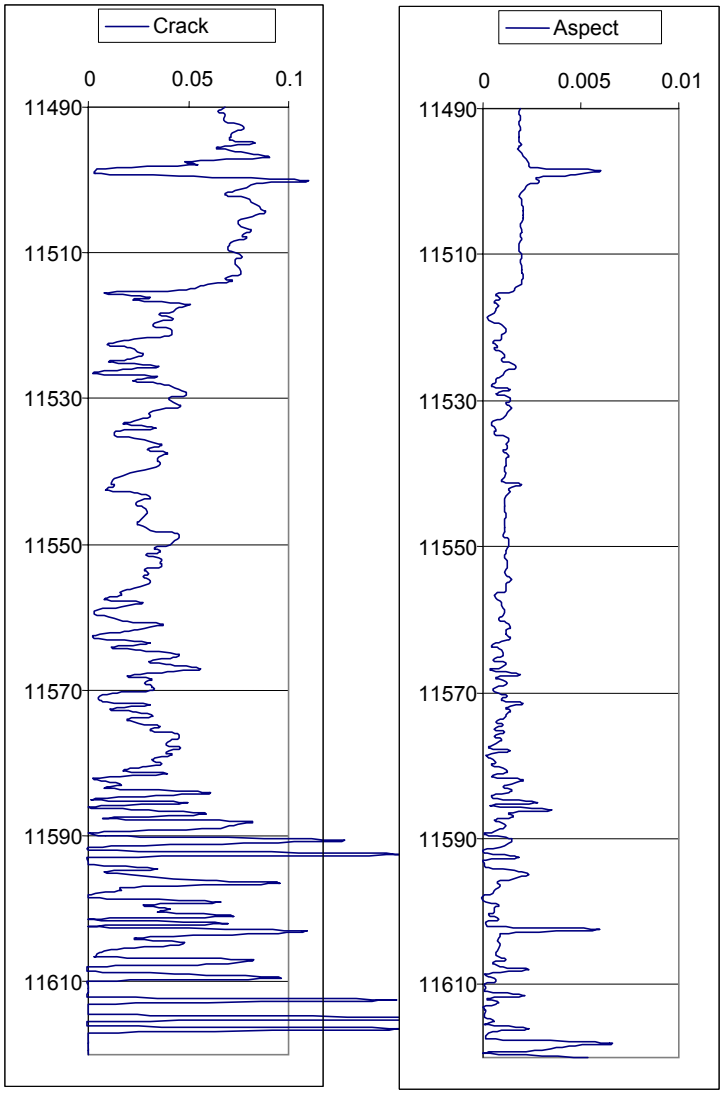

Fig. 7. Synthetic Example Crack Density and Aspect Ratio Logs

The F value computed from Eq. 49 was taken as a fitness value for the generation; smaller values of F are "better" or "more fit" than chromosomes that have higher values for F. A new generation of chromosomes was then created based on the original population according to the following procedure:

- A set of two parents was selected from the population according to their fitness value.
- The two parents were combined randomly to generate two new offspring. These two new chromosomes were evaluated for fitness. A new set of parents was selected, and the process was repeated until a new population of 30 chromosomes was obtained.
- Once the new population was obtained, mutation was applied randomly to some of the chromosomes in the new population at a mutation rate of 0.01.

The process described was repeated for 100 generations. At the end of the 100th generation, if the fitness value of the best chromosome was greater than 0.001, the process was repeated. The optimum solution to the problem was the chromosome with the lowest fitness value amongst all of the 100 generations.

After retesting the algorithm on the synthetic example, the method was applied to a field case. Through another project at the University of Oklahoma, we had a reasonably complete suite of conventional logs for approximately 40 wells in the Bermejo Field in Ecuador. This field is made up of four distinct reservoirs from essentially two formations. The Bermejo North and Bermejo South Basal Tena formation reservoirs are distributary channel sandstones. The Bermejo North and Bermejo South Hollin formation reservoirs are fairly thick fluvial sandstone reservoirs. The Bermejo North and South reservoirs are isolated from each other by high angle reverse faults which form both stratigraphic relief for the trap and the seal for the reservoirs on one side. Between the Basal Tena and Hollin formations there are interbedded shale, sandstone and limestone formations, which have thus far proved unproductive. Figure 8 shows the crack density results from the model for the wells BS-05, BS-14, BS-17 and BS-18. Due to the level of faulting and the structural relief shown in the reservoir, fracturing should be expected. The operator does not feel that any of the reservoirs show naturally fractured behavior. These results need to be compared to the production response in each well to see whether the log-derived crack density and/or aspect ratio are indicating enhanced productivity due to fractures. That work has proved to be both time consuming and difficult in this particular field as the field is in a fairly remote area and data is both sparse and somewhat unreliable.

The difficulty with the O'Connell and Budiansky model is that this model was originally developed for use on core-scale samples. It is not readily clear exactly what the model is calculating when used at a scale consistent with what the log suite is measuring. Additional experimentation is necessary to quantify how to use the model. The plan for this experimentation will be provided following a discussion of another technique that may prove equally promising: that of using fuzzy logic to obtain a "fracturing index" from conventional logs.

The response of conventional well logging tools is affected only indirectly by the presence of fractures. It is through these indirect effects that the fractures may be detected (Serra, 1986). Then in order to "see" fractures from conventional well logs, the available log-suite must be examined quantitatively to distinguish fractures from other features that may produce similar well log responses.

Fuzzy logic is a convenient way to map an input space into an output space when the input variables are related among themselves and with the output variable in a complex but implicit manner. The problem of fracture detection from well logs clearly fits within the fuzzy logic range of applicability.

Many of the problems faced in engineering, science and business can effectively be modeled mathematically. However when constructing these models many assumptions have to be made which are often not true in the real world. Real world problems are characterized by the need to be able to process incomplete, imprecise, vague or uncertain information. There are many other domains which can best be characterized by linguistic terms rather than, directly, by numbers.

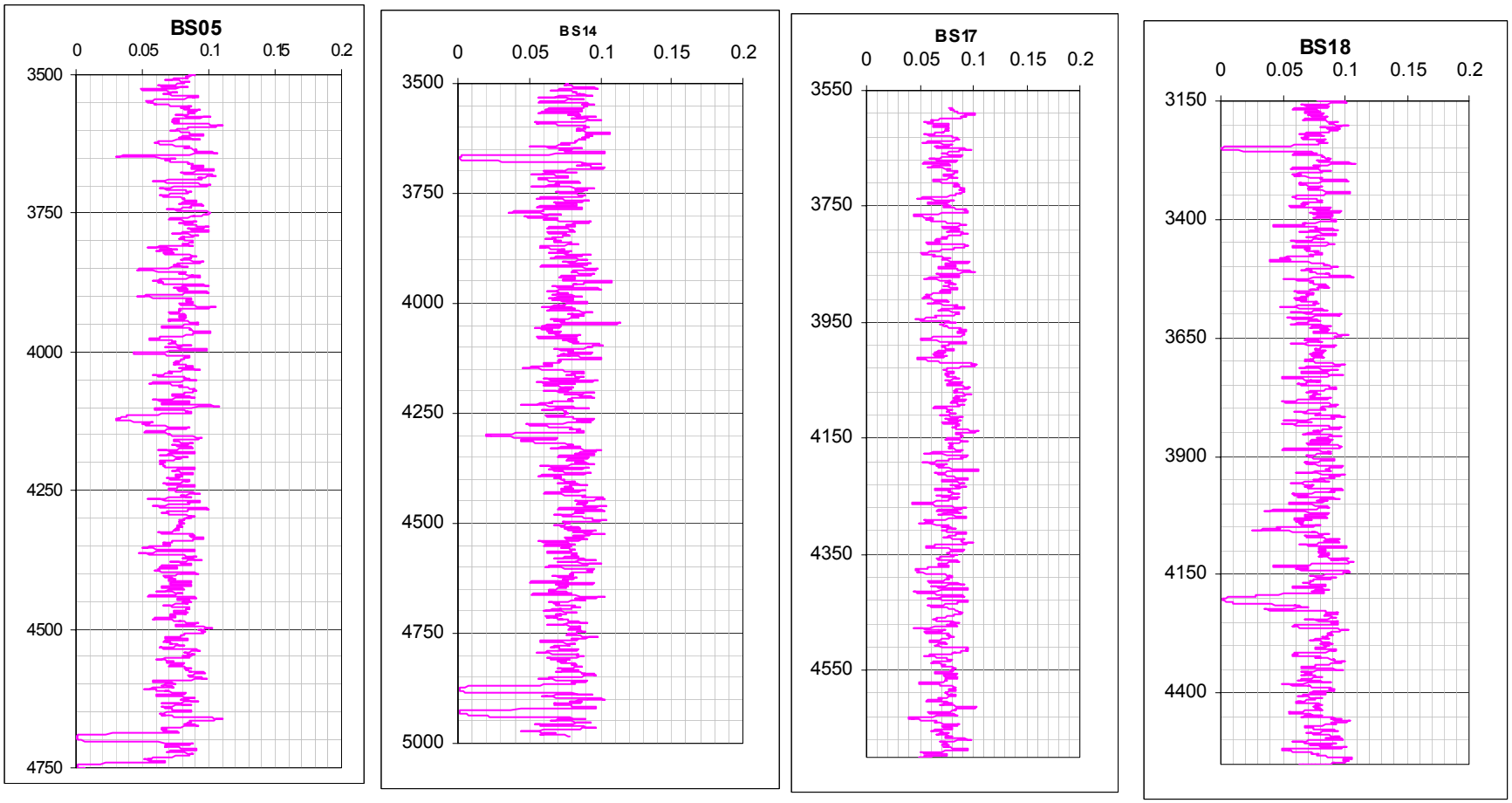

Fig. 8: Bermejo Field Crack Density Logs

Fuzzy sets were introduced by Zadeh (1974) as an approach to handling vagueness or uncertainty and, in particular, linguistic variables. Classical set theory allows for an object to be either a member of the set or excluded from the set. This, in many applications, is unsatisfactory since, for example, if one has the set that describes all males who are tall as those whose height is greater than 5'8" then a 6'0" male is a member of the set. A male whose height is 5'7-3/4", however, is not a member of the set. This implies that a man who is 1/4" shorter than another tall man is not tall.

Fuzzy sets differ from classical sets in that they allow for an object to be a partial member of a set. So, for example, John may be a member of the set 'tall' to degree 0.8. He is tall to degree 0.8. Fuzzy sets are defined by a membership function. For any fuzzy set A the function μ_A represents the membership function for which $\mu_A(x)$ indicates the degree of membership that x, of the universal set X, belongs to set A and is, usually, expressed as a number between 0 and 1:

$$\mu_A(x): X \to [0,1] \quad \text{.....50}$$

Fuzzy sets can either be discrete or continuous. Discrete sets are written as:

$$A = {}^{\mu_1}\!/_{x_1} + {}^{\mu_2}\!/_{x_2} + \cdots + {}^{\mu_n}\!/_{x_n} \quad \text{.....51}$$

where $x_1, x_2, \ldots x_n$ are members of the set A and $\mu_1, \mu_2, \ldots \mu_n$ are their degrees of membership. A continuous fuzzy set A is written as

$$A = \int_X \mu(x)/x \quad \text{.....52}$$

Note that $\int_X$ is not used with its usual meaning. In this case $\int_X$ is the continuous summation of $\mu(x)/x$ over the entire domain.

To be able to deploy fuzzy logic in a rule-based computer system, one needs to be able to handle the operators 'AND' and 'OR' and to be able to carry out inference on the rules. Therefore we need to be able to perform the intersection and union of two fuzzy sets.

The intersection of two fuzzy sets A and B is specified in general by a binary operation on the unit interval; that is, a function of the form

$$i: [0,1] \times [0,1] \to [0,1] \quad \text{.....53}$$

For each element x of the universal set, this function takes as its argument the pair consisting of the element's membership grades in set A and in set B, and yields the membership grade of the element in the set constituting the intersection of A and B. Thus,

$$(A \cap B) = i[A(x), B(x)] \quad \text{.....54}$$

for all $x \in X$

The functions i that qualify as fuzzy intersections must satisfy the following axioms for all $a, b, d \in [0,1]$:

- Axiom 1: $i(a,1) = a$ (boundary condition).

- Axiom 2: $d \geq b$ implies $i(a,d) \geq i(a,b)$ (monotonicity).

- Axiom 3: $i(a,b) = i(b,a)$ (commutativity).

- Axiom 4: $i(a, i(b,d)) = i(i(a,b), d)$ (associativity).

Functions that satisfy these axioms are called t-norms. Examples of some t-norms that are frequently used as fuzzy intersections (each defined for all $a,b \in [0,1]$) are:

- Standard intersection: $i(a,b) = \min(a,b)$

- Algebraic product : $i(a,b) = ab$.

- Bounded difference : $i(a,b) = \max(0, a + b - 1)$

Like fuzzy intersection, the union of two fuzzy sets A and B is specified in general by a binary operation on the unit interval; that is, a function of the form

$$u : [0,1] \times [0,1] \to [0,1] \quad \text{.....55}$$

For each element x of the universal set, this function takes as its argument the pair consisting of the element's membership grades in set A and in set B, and yields the membership grade of the element in the set constituting the union of A and B. Thus,

$$(A \cup B)(x) = u[A(x), B(x)] \quad \text{.....56}$$

for all $x \in X$.

The functions u that qualify as fuzzy intersections must satisfy the following axioms for all $a, b, d \in [0,1]$:

- Axiom 1: $u(a,0) = a$ (boundary condition).

- Axiom 2: $d \geq b$ implies $u(a,d) \geq u(a,b)$ (monotonicity).

- Axiom 3: $u(a,b) = u(b,a)$ (commutativity).

- Axiom 4: $u(a, u(b,d)) = u(u(a,b), d)$ (associativity).

Functions known as t-conorms satisfy all the previous axioms. The following are examples of some t-conorms that are frequently used as fuzzy unions (each defined for all $a,b \in [0,1]$).

- Standard union: $u(a,b) = \max(a,b)$

- Algebraic sum: $u(a,b) = a + b - ab$.

- Bounded sum: $u(a,b) = \min(1, a + b)$

The most widely adopted t-norm for the union of two fuzzy sets A and B is the standard fuzzy union, and for the intersection of two fuzzy sets A and B is the standard fuzzy intersection.

The truth value of a fuzzy proposition is obtained through fuzzy implication. In general a fuzzy implication is a function of the form:

$$\vartheta : [0,1] \times [0,1] \Rightarrow [0,1] \quad \text{.....57}$$

which for any possible truth values a,b of given fuzzy propositions p, q, respectively, defines the truth value, $\vartheta(a,b)$, of the conditional proposition "IF p, THEN q". There are several accepted ways to define ϑ. One way is defining ϑ as:

$$\vartheta(a,b) = u[c(a),b] \quad \text{.....58}$$

for all $a,b \in [0,1]$, where u and c denote a fuzzy union and a fuzzy complement, respectively. According to the previous definition for fuzzy implication, it is possible to obtain infinite expressions for fuzzy implication depending upon the selection of the fuzzy union and the fuzzy complement, particularly, for the standard fuzzy union and the standard fuzzy intersection we have:

$$\vartheta(a,b) = \max(1-a,b) \quad \text{.....59}$$

The family of fuzzy implication relations obtained from this implication definition are called the S implications.

Another implication definition widely accepted is given by:

$$\vartheta(a,b) = \sup\{x \in [0,1] \mid i(a,x) \le b\} \quad \text{.....60}$$

Again, depending on the selection for the fuzzy implication is possible to obtain different fuzzy implication equations, they are usually called R implications.

Essentially the advantage of a fuzzy set approach is that it can usefully describe imprecise, incomplete or vague information. However, being able to describe such information is of little practical use unless we can infer with it. Assuming that there is a particular problem that cannot (at all or with difficulty) be tackled by conventional methods such as by developing a mathematical model, after some process (e.g. knowledge acquisition from an expert in the domain) the 'base' fuzzy sets that describe the problem are determined. The rules (usually of an IF....THEN.... nature (if-then)) are thus determined. These rules then have to be combined in some way referred to as rule composition.

Finally conclusions have to be drawn - defuzzification. There are variations on this approach but essentially we can define a Fuzzy Inference System (FIS) as:

- The base fuzzy sets that are to be used, as defined by their membership functions;

- The rules that combine the fuzzy sets;

- The fuzzy composition of the rules;

- The defuzzification of the solution fuzzy set.

All these components of a FIS present complex, interacting choices that have to be made. The rest of this section describes each component in turn and discusses the various approaches that have been used to aid the FIS developer.

As described earlier, a fuzzy set is fully defined by its membership function. How best to determine the membership function is the first question that has to be addressed. For some applications the sets that will have to be defined are easily identifiable. For other applications they will have to be determined by knowledge acquisition from an expert or group of experts. Once the names of the fuzzy sets have been established, one must consider their associated membership functions.

The approach adopted for acquiring the shape of any particular membership function is often dependent on the application. In some applications membership functions will have to be selected directly by the expert, by a statistical approach, or by automatic generation of the shapes. The determination of membership functions can be categorized as either being manual or automatic. The manual approaches just rely on the experience of an expert and his/her subjective judgment. All the manual approaches suffer from the deficiency that they rely on very subjective interpretation of words.

The automatic generation of membership functions covers a wide variety of different approaches. Essentially what makes automatic generation different from the manual methods is that either the expert is completely removed from the process or the membership functions are 'fine tuned' based on an initial guess by the expert. The emphasis is on the use of modern soft computing techniques (in particular genetic algorithms and neural networks).

As has already been seen, the fuzzy set approach offers the possibility of handling vague or uncertain information. In a fuzzy rule-based system the rules can be represented in the following way:

- If (x is A) AND (y is B)……AND…..THEN (z is Z)

where x, y and z represent variables (e.g. distance, size) and A, B and Z are linguistic variables such as far, near, or small. The process of rule generation and modification can be done manually by an "expert," or automatically using neural networks or genetic algorithms.

Aggregation is the process by which the fuzzy sets that represent the outputs of each rule are combined into a single fuzzy set. The input of the aggregation process is the list of truncated output functions returned by the implication process for each rule. The output of the aggregation process is one fuzzy set for each output variable.

Given a set of fuzzy rules the process is as follows:

- For each of the antecedents find the minimum of the membership function for the input data. Apply this to the consequent.

- For all rules construct a fuzzy set that is a truncated set using the maximum of the membership values obtained.

Once the rules have been composed the solution, as has been seen, is a fuzzy set. However, for most applications there is a need for a single action or crisp solution to emanate from the inference process. This will involve the defuzzification of the solution set. There are various techniques available. Lee (1990) describes the three main approaches as the max criterion, mean of maximum and the center of area.

The max criterion method finds the point at which the membership function is a maximum. The mean of maximum takes the mean of those points where the membership function is at a maximum. The most common method is the center of area method, which finds the center of gravity of the solution fuzzy sets. For a discrete fuzzy set this is

$$\frac{\sum_{i=1}^{n} u_i d_i}{\sum_{i=1}^{n} u_i} \quad \text{.....61}$$

where d_i is the value from the set that has a membership value u_i. There is no systematic procedure for choosing a defuzzification strategy.

Application to Well Logs

Several of the most commonly recorded conventional well logs, (i.e., Caliper, Gamma Ray, Spontaneous potential, Sonic, Density correction, MSFL, Shallow and deep resistivity), are used in this study to obtain a continuous log of fracture index through a FIS.

In order to accomplish this goal, the original well log data needs to be preprocessed prior to the use of the FIS. Once the data is preprocessed, we proceed to define the membership functions and the implications required by the Fuzzy Inference System in order to obtain a fracture indication index.

The presence of a single fracture or a system of fractures can cause minor to significant departures from the "normal" well log response. Such abnormalities may be recorded by the different logging devices. When analyzing conventional well logs to determine the presence of fractures several aspects have to be taken into account:

- No single tool gives absolute indication of the presence of fractures.

- Conventional logging tools are affected only indirectly by the presence of fractures, and it is only by these indirect effects that the fractures can be detected.

- Abnormal responses of the different logging tools may also be the result of phenomenon not related to fractures.

Caliper Log: Fractured zones may exhibit one of two basic patterns on a caliper log:

- A slightly reduced borehole size due to the presence of a thick mud cake, particularly when using loss circulation material or heavily weighted mud. Suau, (1989).
- Borehole elongation observed preferentially in the main direction of fracture orientation over fracture zones due to crumbling of the fracture zone during drilling.

SP Log: Frequently the SP-curve appears to be affected by fracturing. The response of the SP curve in front of fractured zones has the form of either erratic behaviour or some more systematic negative deflection probably due to a streaming potential (the flow of mud filtrate ions into the formation). However streaming potentials can also occur from silt beds (Crary et al, 1987).

Gamma Ray Log: Radioactive anomalities are recorded by the Gamma Ray log in fractured zones. The observed increase in gamma radioactivity (without concurrently higher formation shaliness) can result from water-soluble uranium salts deposited by connate water along fracture surfaces (Rider, 1986).

Density Log: Since density logs measure total reservoir porosity, fractures often create sharp negative peaks on the density curve. Assuming that more mudcake accumulates at fractures than elsewhere, the $\Delta\rho$ correction curve reacts to this build up as wheel as to the fluid behind the mudcake reporting an anomalous high correction to the density log.

Neutron log: Similar to the density log, any neutron-type log also measures total reservoir porosity in carbonate rocks. A neutron log by itself is not a reliable fracture indicator. However comparison of neutron log response with other porosity logs may be helpful in determining the zones that may be fractured in the reservoir.

Sonic Log: Large fractures, particularly the subhorizontal ones, tend to create “cycle skipping” on the normal transit time curve. This causes the measured travel time to be either too long or too short (Bassiouni, 1994).

Laterlogs: The dual laterlog generally provides three resistivity measures, the deep laterlog, the shallow laterlog and the microspherically focused log (MicroSFL). The MicroSFL, which measures resistivity at the invaded zone, responds with high fluctuations in front of fractures. In fresh muds the deep and shallow laterlogs will qualitatively indicate fractures. The shallow curve, due to its proximity to the current return, is more affected than the deep laterlog, and therefore registers a lower resistivity value.

The preprocessing stage is comprised of two major steps: data filtration step, and the data scaling step. The main objectives of the preprocessing are:

- Reduce random noise in the measurements.
- Scale and normalize the logs within the same range, so they can easily be compared in the Fuzzy inference system.

- Obtain the statistical characteristics of the data in order to design appropriate membership functions.

A filter is a mathematical operator that converts a data series into another data series having prespecified form. A digital filter's output *y(n)* is related to its input *x(n)* by a convolution with its impulse response *h(n)* (Mathworks, 1999):

$$y(n) = h(n)X(n) = \sum_{m=-\infty}^{m=\infty} h(n-m)x(m) \quad \text{.....62}$$

In general, the z-transform, *y(z)* of a digital filter's output *y(n)* is related to the z-transform *x(z)* of the input by:

$$y(z) = H(z)X(z) = \frac{b(0) + b(1)z^{-1} + ... + b(nb)z^{-nb}}{a(0) + a(1)z^{-1} + ... + a(na)z^{-na}} x(z) \quad \text{.....63}$$

where *H(z)* is the filter transfer function. Here, the constants *b(j)* and *a(j)* are the filter coefficients and the order of the filter is the maximum of n_a and n_b. Many standard names for filters reflect the number of *a* and *b* coefficients present:

- When $n_b = 0$ (that is, *b* is a scalar), the filter is an Infinite Impulsive response (IIR)

- When $n_a = 0$ (that is *a* is a scalar), the filter is a finite Impulsive Response (FIR), all zero, non-recursive, or moving average (MA) filter.

- If both n_a and n_b are greater than zero, the filter is an IIR, pole zero recursive, or autoregressive moving average (ARMA) filter.

It is simple to work back to a difference equation from the z-transform relation shown earlier. Assume *a*(1)=1. Move the denominator to the left hand side and take the inverse z transform:

$$y(n) + a_2 y(n-1) + ... + a_{n_{a+1}} y(n-na) = b_1 x(n) + b_2 x(n-1) + ... + b_{n_{b+1}} x(n-n_b) \quad \text{.....64}$$

This is the standard time-domain representation of a digital filter, computed starting with *y*(1) and assuming zero initial conditions. The progression of this representation is:

- $y(1) = b_1 x(1)$

- $y(2) = b_1 x(2) + b_2 x(1) - a_2 y(1)$

- $y(3) = b_1 x(3) + b_2 x(2) + b_3 x(1) - a_2 y(2) - a_3 y(1)$

For sake of simplicity, in this study, a moving average (MA) filter is implemented with different well logs. This moving average is obtained using six data points (3 data points forward and 3 data points backward from the input value) with the same weight. Since the well log data files to be used in this study are digitized every 0.5 ft, the length of the filter is 3 ft, which is

reasonable to detect deviation from the moving average with wavelengths of the order of inches (as might be expected for discrete fractures).

Since fractures are correlated with anomalies in well logs, this six point moving average is used as a "background" value to which each data point is compared. The entire population of deviations from the background is then used to design membership functions. Depending on which well log is being considered, either positive, negative, or absolute deviations from background are significant:

Sonic log: Only differences which represent an increase in sonic transit time, relative to the background transit time, are significant when considering the influence of fractures on the sonic log.

Caliper: Only positive deviations from background value may indicate the presence of fractures.

MicroSFL: Since the response of this tool fluctuates dramatically in front of fractures, both, positive and negative deviations from background value are significant.

Natural gamma ray: Only positive deviations from background are significant when considering the influence of fractures on this log.

Spontaneous potential: The erratic response that this log may exhibit in the presence of fractures makes both positive and negative deviations from background value important.

Density correction: Only positive deviations from background value are important.

Resistivity logs: In this case, since shallow and deep resistivity logs need to be analyzed together, a different procedure must be implemented. Fracture detection with these logs is based on the principle that a logging tool, which looks deep into the rock mass, is less influenced by fractures than a shallow reading device (Schlumberger Ltd., 1989). In vertical fractures, the shallow resistivity log will register a lower resistivity. The procedure followed to incorporate resistivity logs in the fracture detection algorithm are summarized in the following steps:

- Take the ratio between the shallow and deep reading tools.

- Subtract this ratio from a background value.

- The presence of fractures may be indicated by a high positive deviation from background.

Data scaling is necessary for two reasons. First, it is desired to account for essential variability in the filtered log data, and, without some type of scaling process, those logs with the largest original variance would dominate the subsequent analysis. Second, it is desired to have all logs measured in similar units.

In this study a linear scaling method that maps the maximum log value to one and the minimum log value to zero will be used. The linear scaling has the following form:

$$z_i = \frac{x_i - a}{b} \quad \text{.....65}$$

where z_i is the scaled value, x_i is the original value, a and b are scaling constants.

Once each well log is filtered and scaled, the next step is to define the membership functions. Two membership functions have been designed for each well log. Each membership function maps the universe of discourse (in this case, the entire preprocessed curve) to a fuzzy subset, which expressed whether the probability of fractures is high or low.

Membership functions are designed for each log according to the significance of the deviation from background value to the presence of fractures. Two cases are identified:

(a) When positive deviation from background may be related to fractures (sonic, caliper, and gamma ray and resistivity logs). In this case a sigmoidal membership function will be used. This membership function is defined as (Roger et al, 1997):

$$sig(x;a,c) = \frac{1}{1+\exp(-a(x-c))} \quad \text{.....66}$$

where a is the slope at the crossover point, $x = c$.

Depending on the sign of the parameter a, a sigmoidal MF is inherently open right or left. An open right sigmoidal MF indicates high likehood of fractures, while an open left sigmoidal MF indicates low likehood of fractures. The crossover point is assumed to be the mean plus one standard deviation of the data. The form that the final MF takes is shown in Figure 9.

(b) When absolute deviations from background may be related to a high probability of fractures as in the spontaneous potential and MSFL logs, the generalized bell MF seems to be appropriated. A generalized bell MF is specified by three parameters (Roger et al, 1997)

$$bell(x;a,b,c) = \frac{1}{1+\left|\frac{x-c}{a}\right|^{2b}} \quad \text{.....67}$$

where c represents the MFs center, a determines the MF width, and, b is an additional parameter related to the slope at the point $c+a$.

The center and width of the MF is taken as the mean and standard deviation of the data, respectively. The form that the final MF takes is shown in Figure 10. The membership function for the output variable-fracture index will indicate the probability of fractures according to the logs analyzed. In this case, sigmoidal membership functions are used to indicate high and low fracture index.

To apply FIS to fracture identification the rules need to be set. Among the rules that are being used to obtain a fracture intensity index from conventional well logs are:

- If (caliper is high) and (sonic is high) then (fracture index is high).

- If (resistivity is high) and (MSFL is high) then (fracture index is high).

The number of rules necessary to fully specify output variables for all input variables is given by S^*n, where S is the number of fuzzy subsets assigned to the input variables and n is the number of input variables.

Figure 11 shows three of the Fuzzy Inference Process rules used have been put together to show how the output of each rule is combined into a single fuzzy set, and finally the output fuzzy set was defuzzified using the centroid calculation method which returns the center of area under the curve.

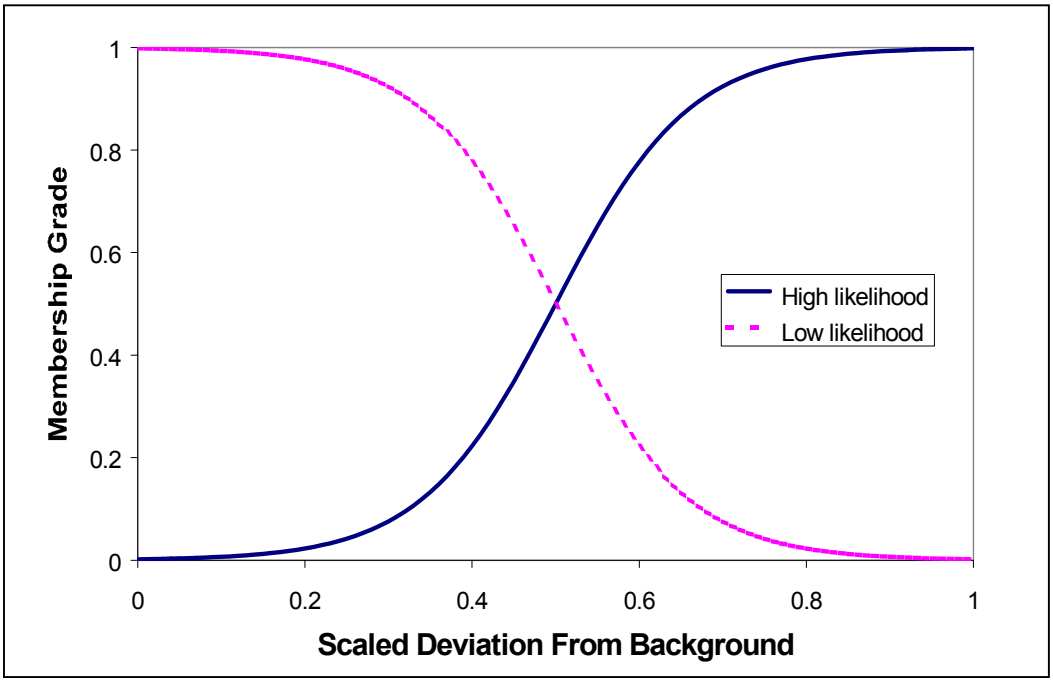

Figure 9: Sigmoidal Membership Function

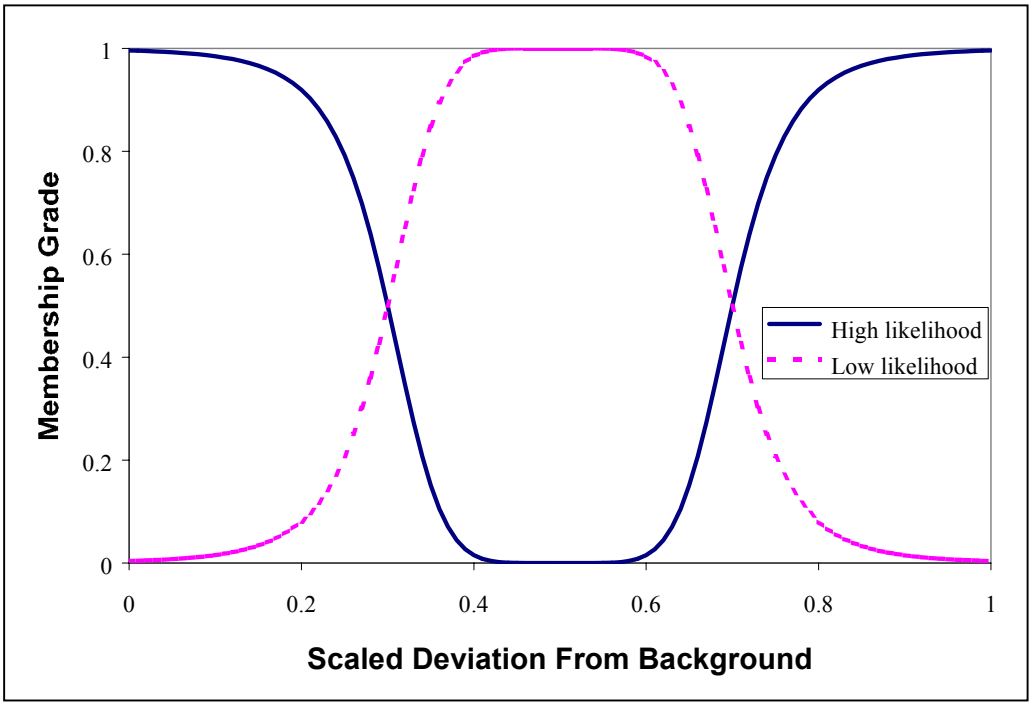

Figure 10: Generalized Bell Membership Function

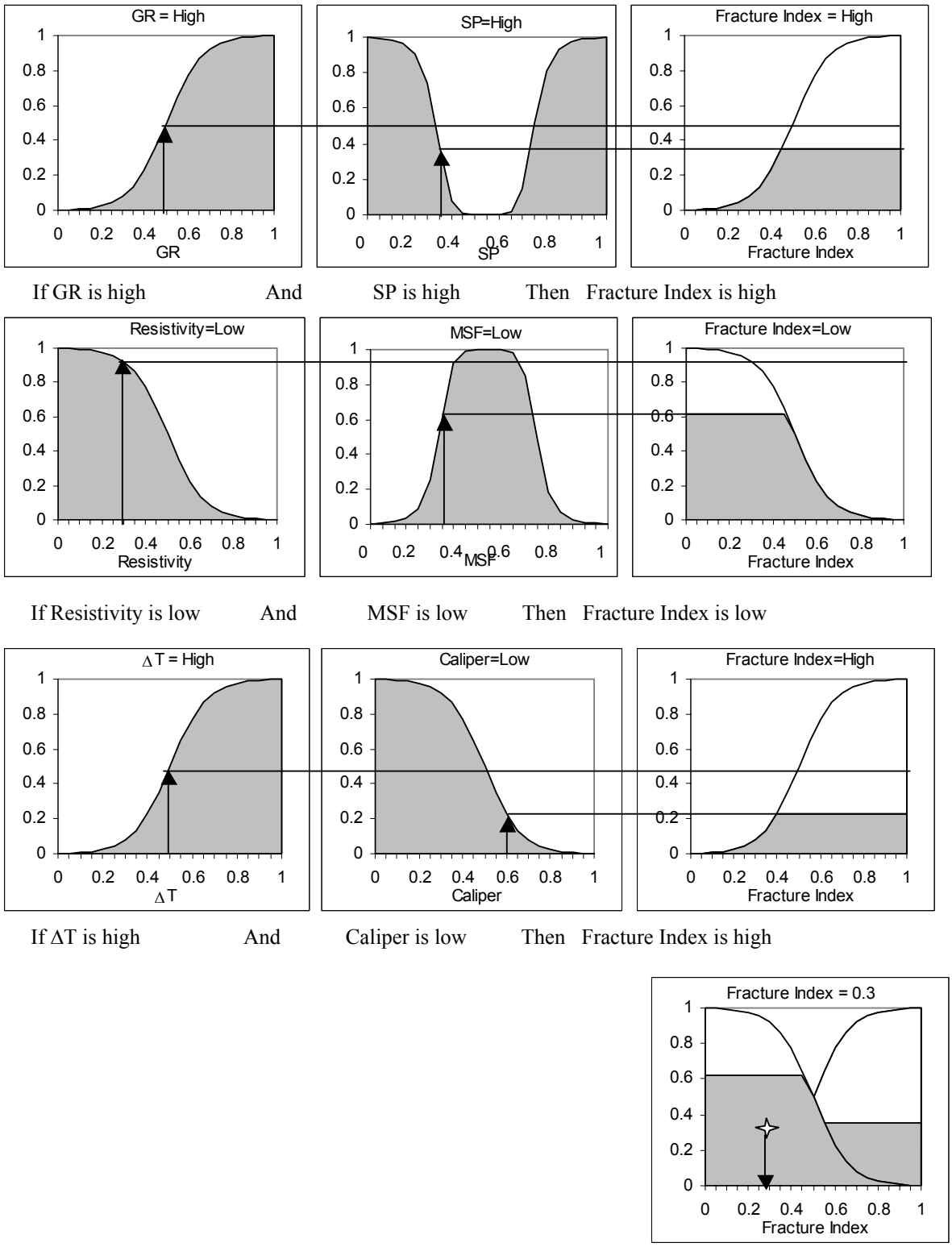

Figure 11: Fuzzy Inference Process

The data studied in this example include a full set of conventional well logs run in the Bermejo field in Ecuador. The Fracture index logs obtained for the wells analyzed are presented in Figure 12 and 13.

Again, a more detailed analysis of exactly what the fracture index and what the crack density and aspect ration are indicating needs to be quantified. To that end, geologic characterizations of cores from the Frontier formation in Wyoming, the Mesa Verde formation in Colorado and the Austin Chalk formation in Texas were obtained from John Lorenz at Sandia National Labs. After contacting the current operator of the wells, the only logs available were for a well in the Austin Chalk formation.

Boreholes that are suitable for case study are rare. In order to apply the Fuzzy Inference Algorithms, several conventional well logs that are useful for fracture detection must be available, and in order to apply O'Connell and Budiansky inverse algorithm, the suite of logs available must be complete enough to allow for the calculation of the lithology and saturations. Data quality must be carefully examined since reliable log information cannot be obtained under adverse borehole conditions. Additionally, some calibration of the log results to actual data is recommended. In order to do so, the borehole must either be continuously cored, or contain a detailed imaging log that can be used for comparison.

The Mills-McGee well #1 is located in Milam County, TX in the Giddings field (Figures 14 and 15). The Giddings (Austin Chalk-3) Field produces from the Cretaceous Austin Chalk formation. (Rail Road Commission of Texas, 1997). In the area of the well, the formation produces from fine-grained limestone and chalk. Productivity and fluid flow directions are predominantly controlled by the presence of fractures.

High quality geological and geophysical data was acquired for the Mills-McGee #1 well. This well was drilled by The Union Pacific Resources and is now operated by Anadarko Petroleum Corporation. The well had a comprehensive suite of state-of-the-art logs and 220 ft of core was obtained. The well log data was provided to this study in digital format. Well logs used in this study are listed in Table 2. Only those logs that are known to be affected by the presence of fractures were chosen for this analysis. The original well log data is displayed in Figures P–R. Special core analysis characterizing the natural fractures for the well was provided by Lorenz (1997).

Lorenz (1997) describes two categories of fractures that were recognized in the Mills McGee #1 well: 1) "Hairline fractures, which are healed, fully mineralized fractures 0.1mm or less in width; 2) Semi-open fractures which are somewhat wider than hairline fractures. These two fracture types occur in the same zones and are not naturally exclusive. They are inferred to be components of a single fracture population since they have similar characteristics. Unfortunately mechanically induced fractures were identified from the cores but excluded from the analysis.

The caliper log displayed in Figure 16(a) shows that although this is a well in a fractured formation, the borehole does not present any enlargement in the zone between 5860 and 6040ft. The good borehole condition makes the well log measurements very reliable.

The conventional SP log is presented in Figure 16(b). It is possible to observe several zones with an erratic SP behavior presumably due to the presence of fractures.

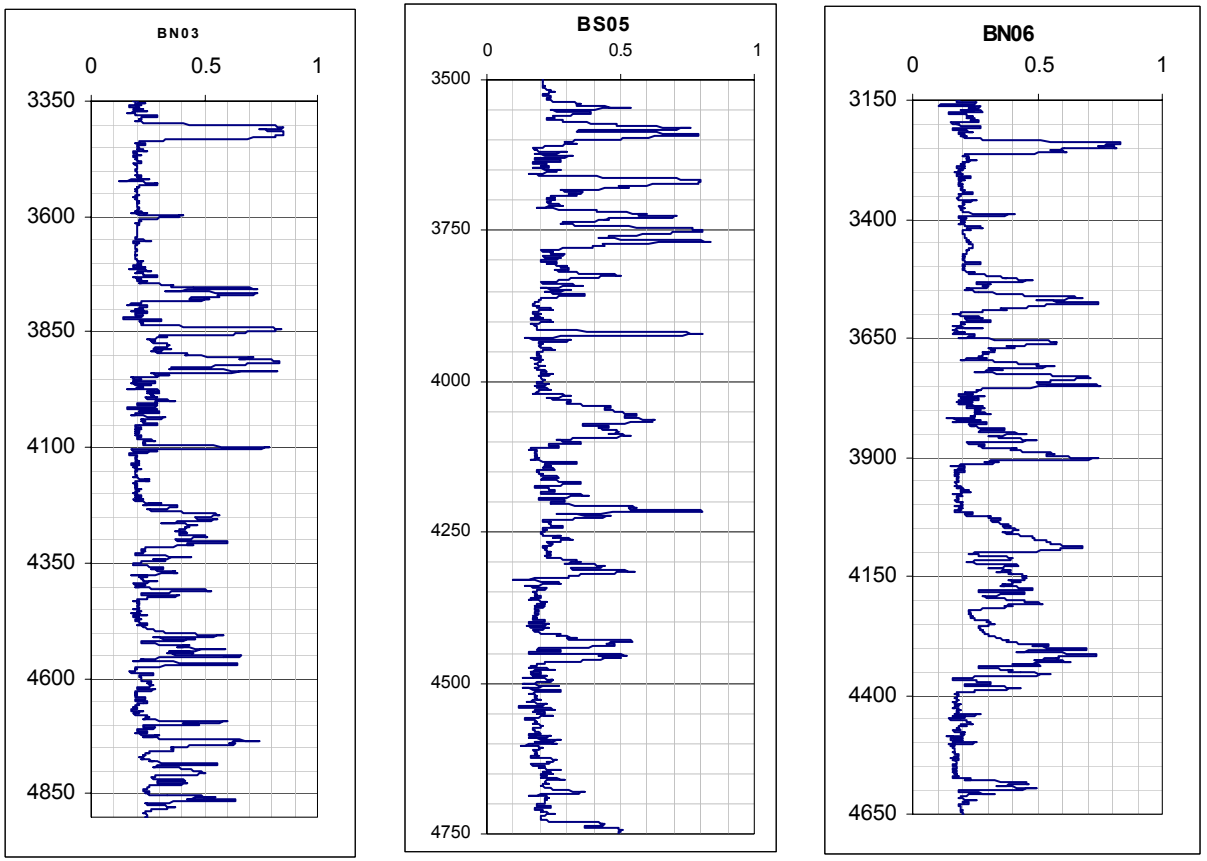

Figure 12: Fracture Index Logs BN-03, BN-05 and BN-06

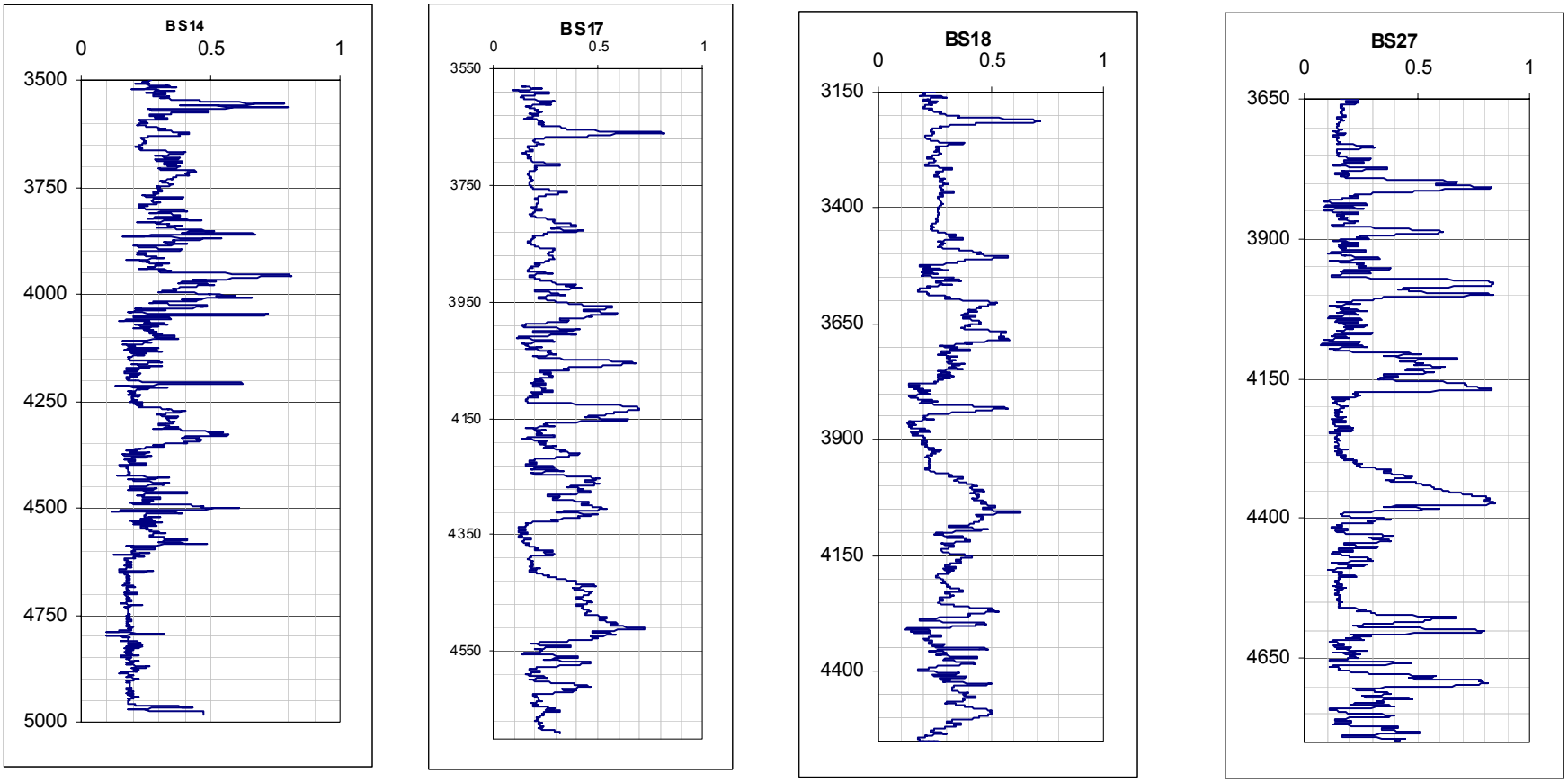

Figure 13: Fracture Index Logs BS-14, BS-17, BS-18 and BS-27

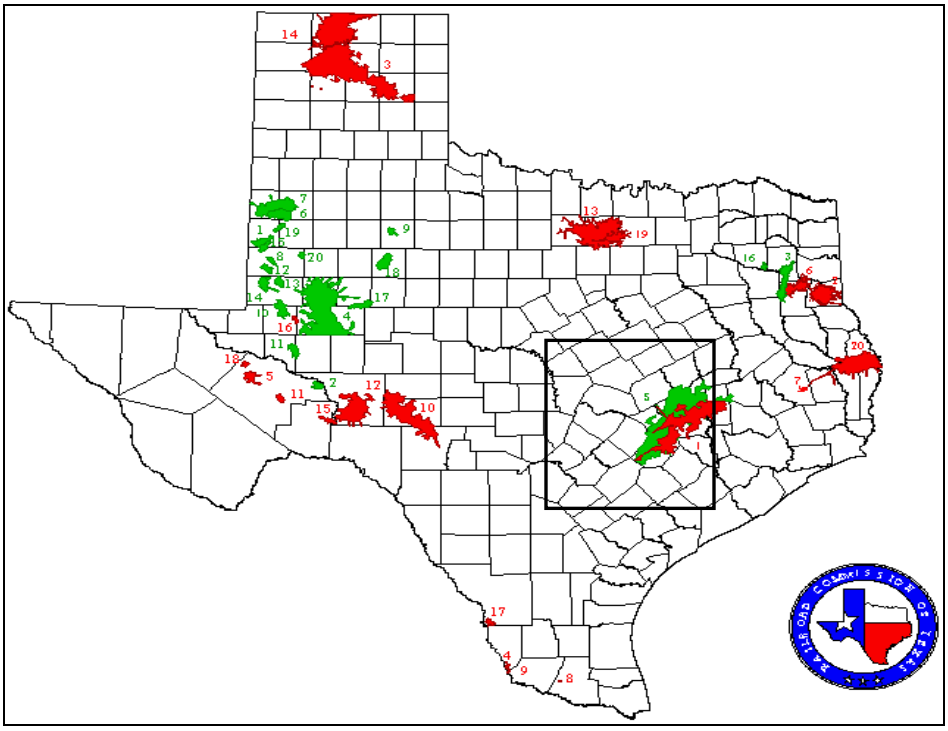

Figure 14: Top Producing Oil and Gas Fields in Texas

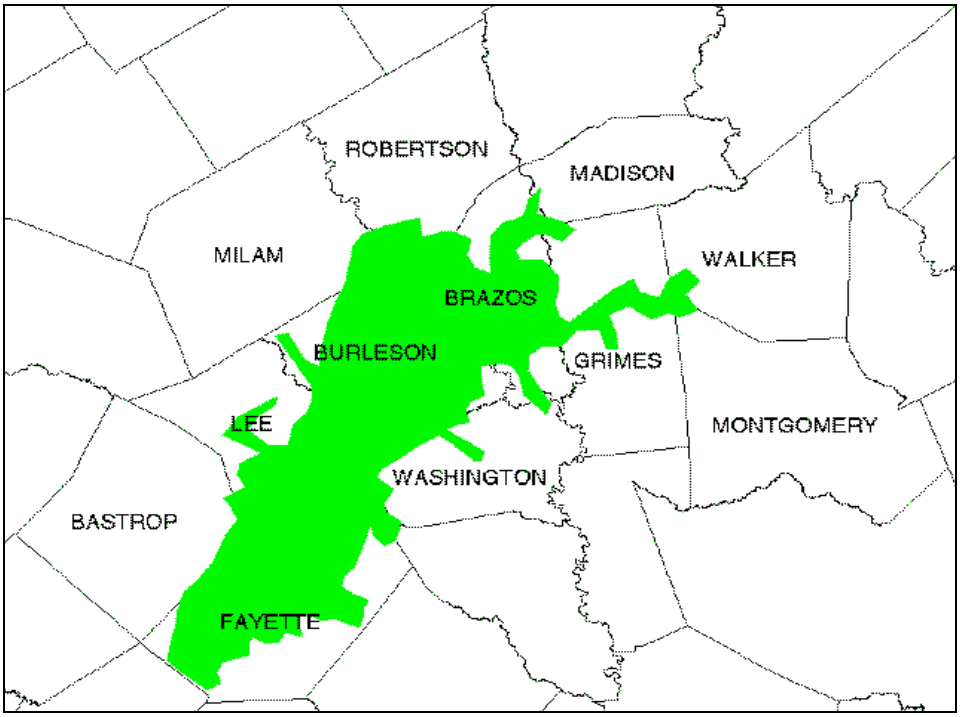

Figure 15: Giddings (Austin Chalk - 3) Field Map

The behavior of the gamma ray log as shown in Figure 16(c) is not a conclusive fracture indicator. The peaks that this log displays in the interval between 5870ft and 6010ft might be due to thin shale beds or to the presence of fractures.

Figure 16(d) shows the sonic log, in this case cycle skipping is not clearly observed, and the compresional travel time values are those corresponding to chalk/shale lithology.

Neutron porosity and density porosity are presented in Figure 17(a). In this case the density porosity value does not report high changes. On the other hand, the neutron porosity is not as smooth as the density porosity, possibly due to the presence of fractures.

Figures 17(b) and 17(c) present the density and density correction logs. The density log reports an almost constant value of bulk density in the interval between 5870 and 6070ft., however, the density correction log reports high correction values in the interval between 5850 and 5940ft. Since the caliper in this interval reports a gauge hole, the abnormalities in the density correction values may be due to the presence of fractures in this interval.

Table 2: Well Logs available for the Mills McGee Well #1

Well logs	Fracture detection significance
Caliper	Registers borehole enlargement that may be caused by the presence of fractures.
Spontaneous Potential	It may indicate the presence of fractures, but, it is not consider a reliable fracture detection tool. (Schlumberger Ltd., 1989)
Gamma Ray	Without the spectral gamma ray data, the gamma ray log by itself is not conclusive in fracture detection.
Bulk Density	Open fractures filled with drilling fluid may cause a reduction in bulk density (Fertl, et al, 1980).
Density correction	It is considered one of the best fracture detection tools among the conventional well logs (Serra, 1986)
Photoelectic factor	Has been recognized as a useful fracture detection tool (Schlumberger Ltd, 1989)
Sonic transit time	Fractures are know to cause cycle skipping (Bassiouni, 1994)
Shallow/Deep Induction combination	The resistivity of the deep induction tool will exceed the one for the shallow induction tool
Spherically Focused Log	Often exhibits erratic values in the presence of fractures, but is sensitive to poor borehole conditions. (Schlumberger, 1987)

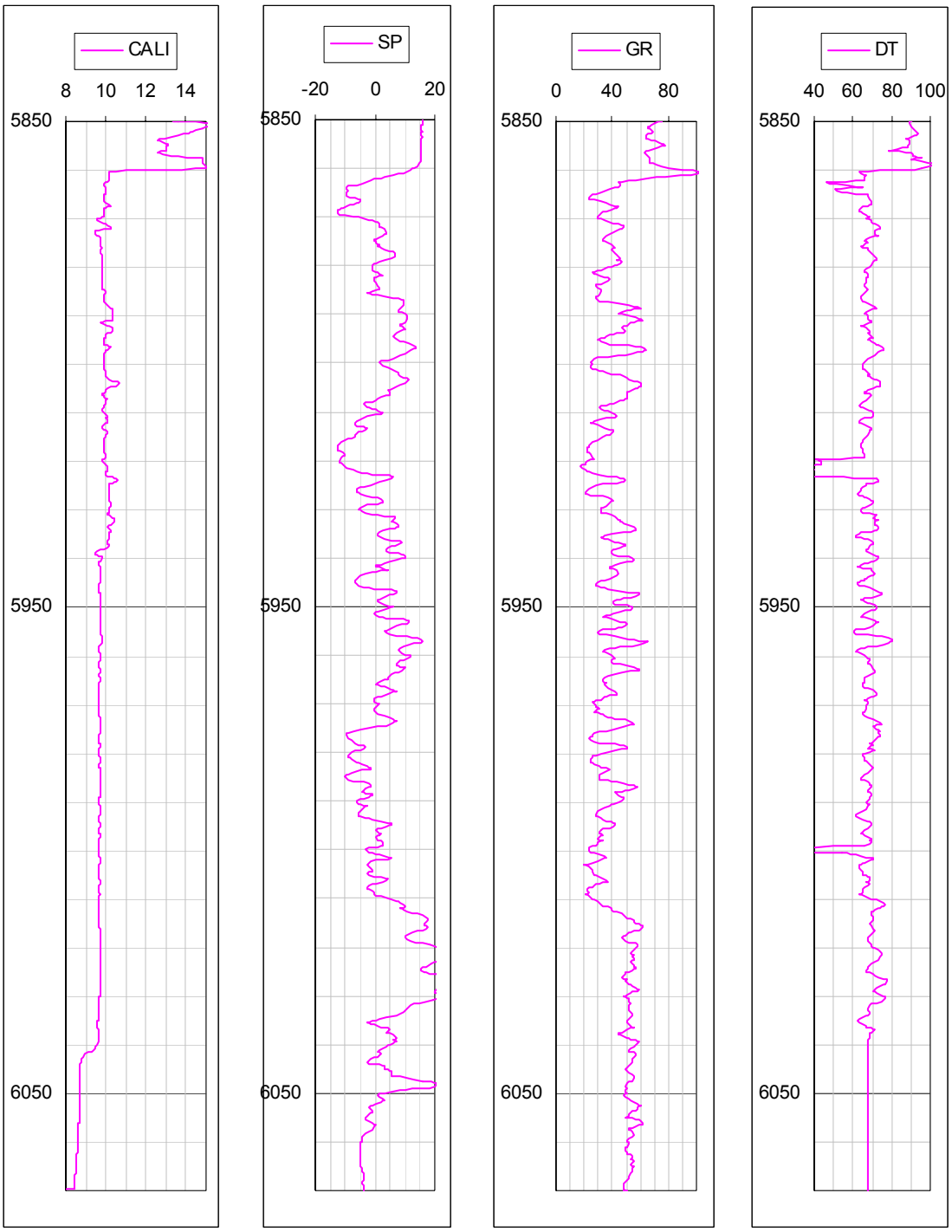

(a) **(b)** **(c)** **(d)**

Figure 16: (a) Caliper, (b) SP, (c) Gamma Ray and (d) Δt logs

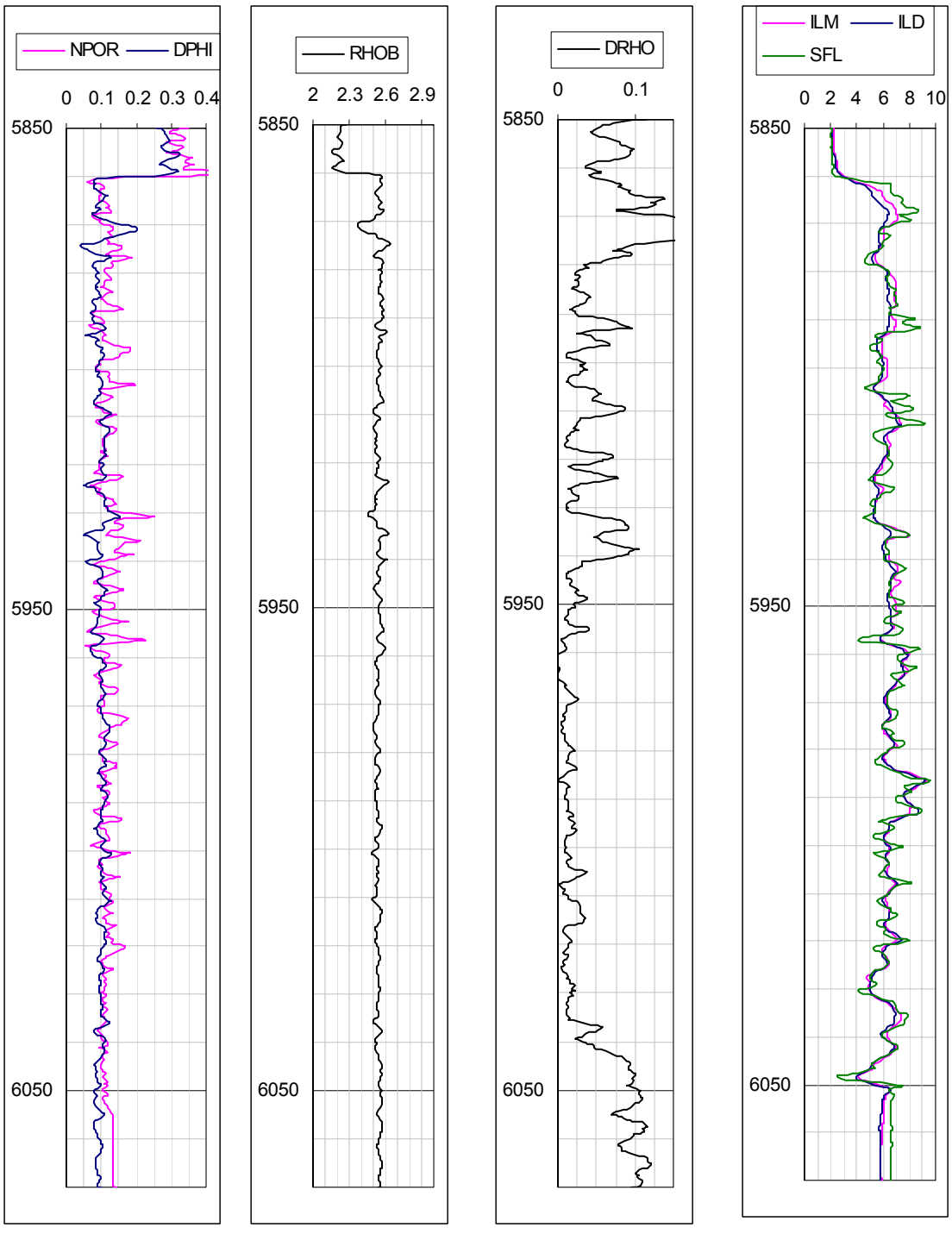

(a) **(b)** **(c)** **(d)**

Figure 17: (a) Neutron and Density Porosities, (b) Bulk Density, (c) Δ Bulk Density and (d) Resistivity Logs

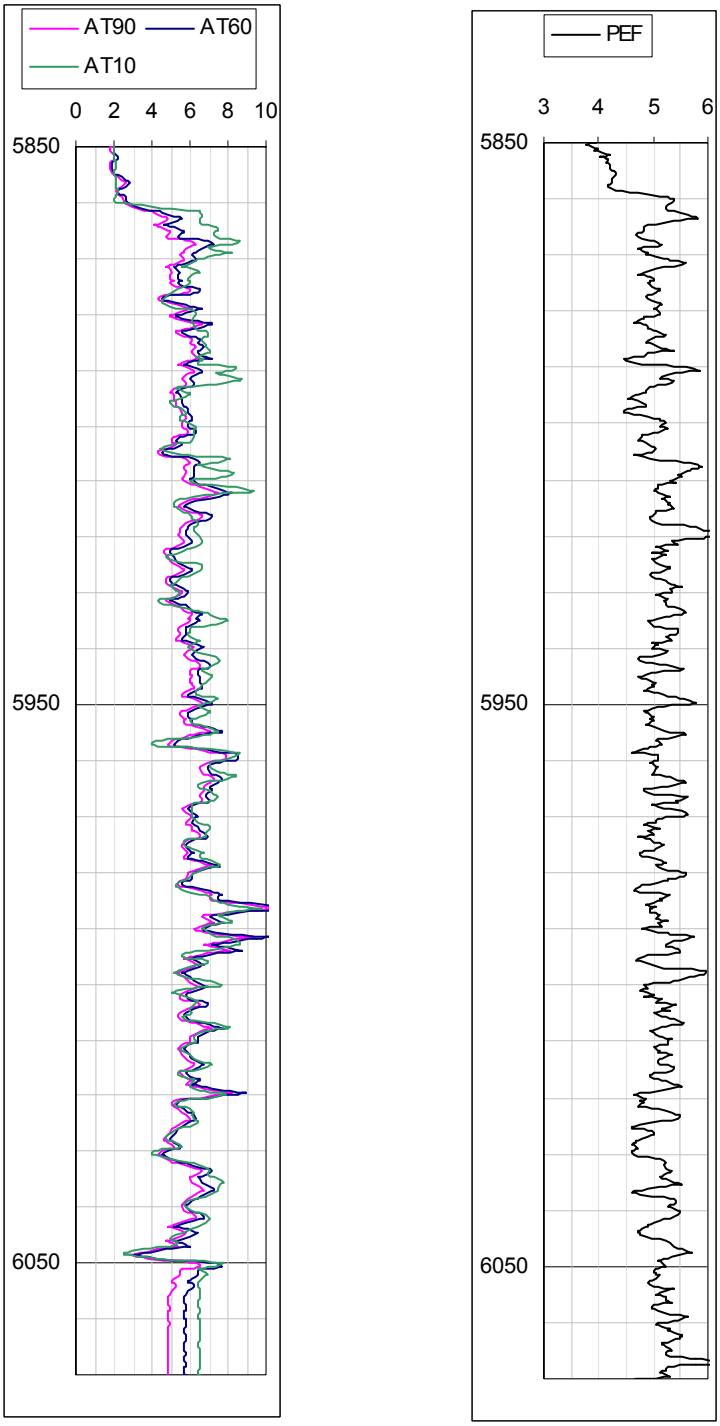

(a) **(b)**

Figure 18: (a) Induction and (b) PEF logs

Figure 17(d) presents the resistivity logs; AT10, AT60, and AT90. AT10 is the shallow resistivity log while AT90 is the deep resistivity log. It is possible to observe some separation between the shallow and deep resistivity logs, especially between 5860 and 5920ft., however in general, in the interval analyzed, there is no significative separation between the two resistivity measurements.

Induction logs are shown in Figure 18(a). In fractured formations these logs indicate the presence of fractures if the SFL (spherically focused log) reads less than the ILD (deep induction log); according to this criteria, it is possible to distinguish several fractured zones in this interval.

The photoelectrical index log is shown in Figure 18(b). This log reports a fairly constant value in the range between 4.5 and 5.5, which is in agreement with the lithology expected in this well.

No individual log shows fracturing directly, but through the use of the FIS, it is possible to infer the presence of fractures in the well analyzed. The processed logs used in the Fuzzy Inference System are shown in Figures 19–21, along with the locations of open and semi-open fractures reported in the core analysis.

The FIS was applied under six different scenarios (set of rules). Figures 22–23 report the results obtained for the different cases. The rules for each one of the cases are presented in Table 3. Each set of rules is defined arbitrarily based on the discussion about the effects of fractures on the different logs presented previously.

Figures 24(a–c) present the results obtained using O'Connell and Budiansky inverse model. Figure 24(d) combines the results obtained for Case 6 of the FIS (the scale has been reduced from 0-1 to 0-0.01), and the fracture porosity.

The fractures reported by the core description are displayed in the figures as dots. Only open and semi open fractures are shown. Hairline fractures are not displayed because they are very numerous, most of them are sealed, and they are not analyzed in the core description.

From the caliper log, it is possible to say that the borehole does not present any major enlargement due to fractures; this fact makes the suit of logs more reliable for the analysis.

For the six cases analyzed using FIS, there is good correlation between the fracture detection algorithm and the core analysis, specifically in the interval between 5910 and 5930 ft. All the cases presented in Figures 22–23, are able to recognize that interval as one with high fracture presence.

The correlation between the core analysis and the log analysis for the set of fractures between 5965 and 5990 ft is not as clear. The only case that is detecting this fractured zone is Case 3, however this case has a high noise level, which makes this combination of rules poorly suited for a FIS for fracture detection.

Case 5 does not seem to be the most appropriate set of rules for the fracture detection algorithm. This indicates then, that caliper, gamma ray and spontaneous potential logs are not conclusive tools for fracture detection.

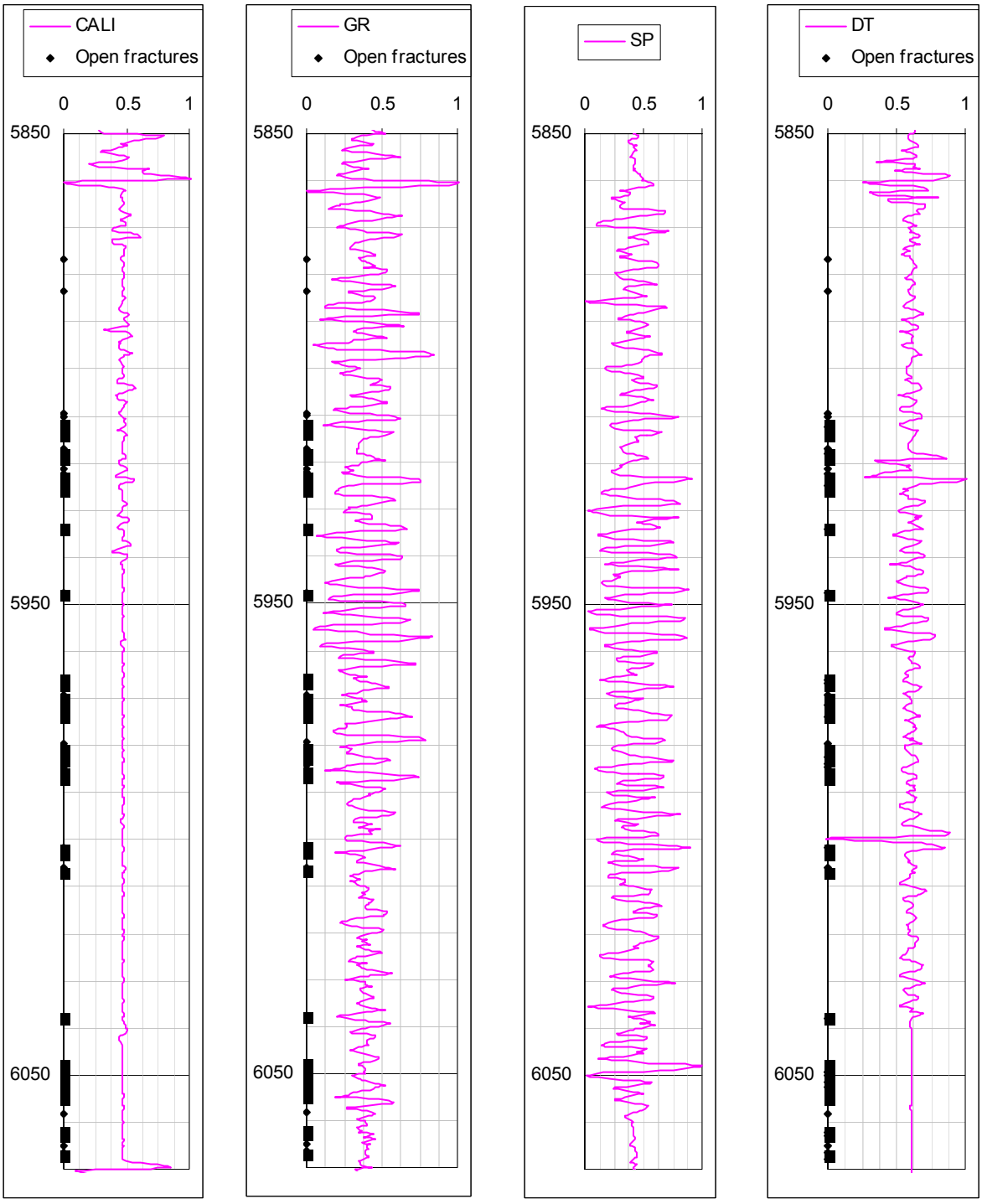

Figure 19: Processed Logs (a) Caliper, (b) Gamma Ray, (c) SP and (d) Sonic Travel Time

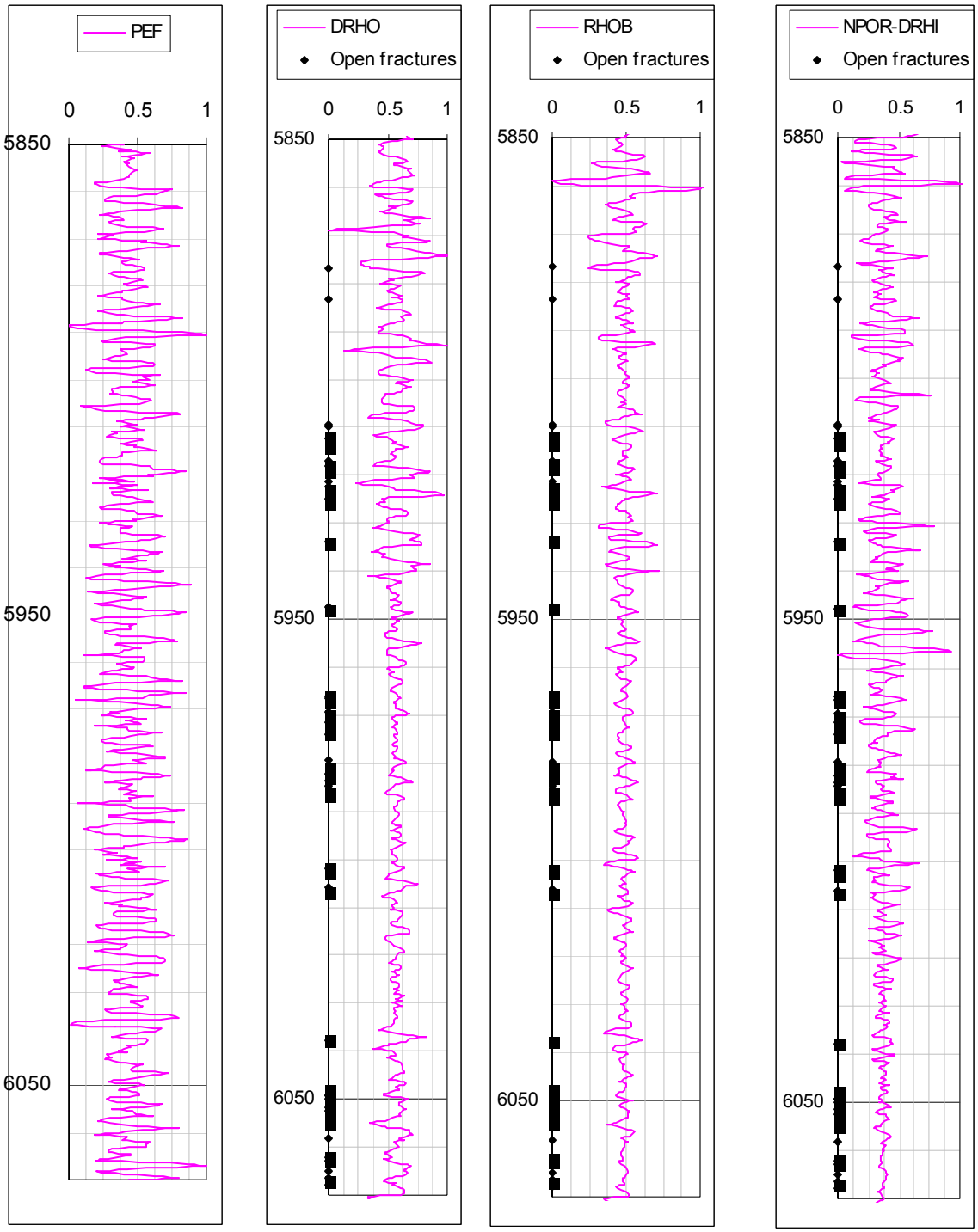

Figure 20: Processed Logs (a) PEF, (b) Δ Bulk Density, (c) Bulk Density, (d) Neutron Porosity – Density Porosity

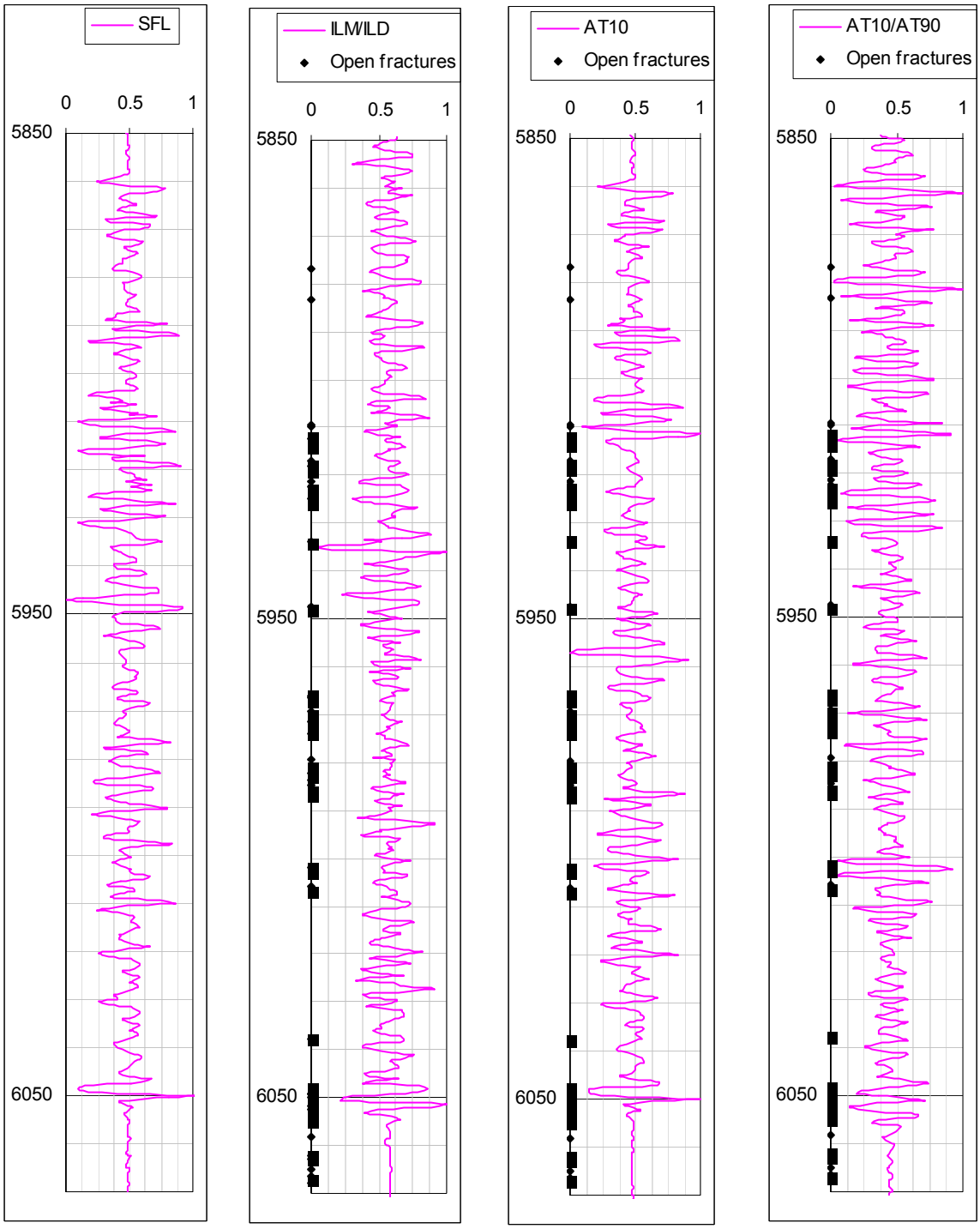

Figure 21: Processed Logs (a) SFL, (b) Medium to Deep Ratio, (c) Shallow Induction and (d) Shallow Induction log to Deep Induction log ratio

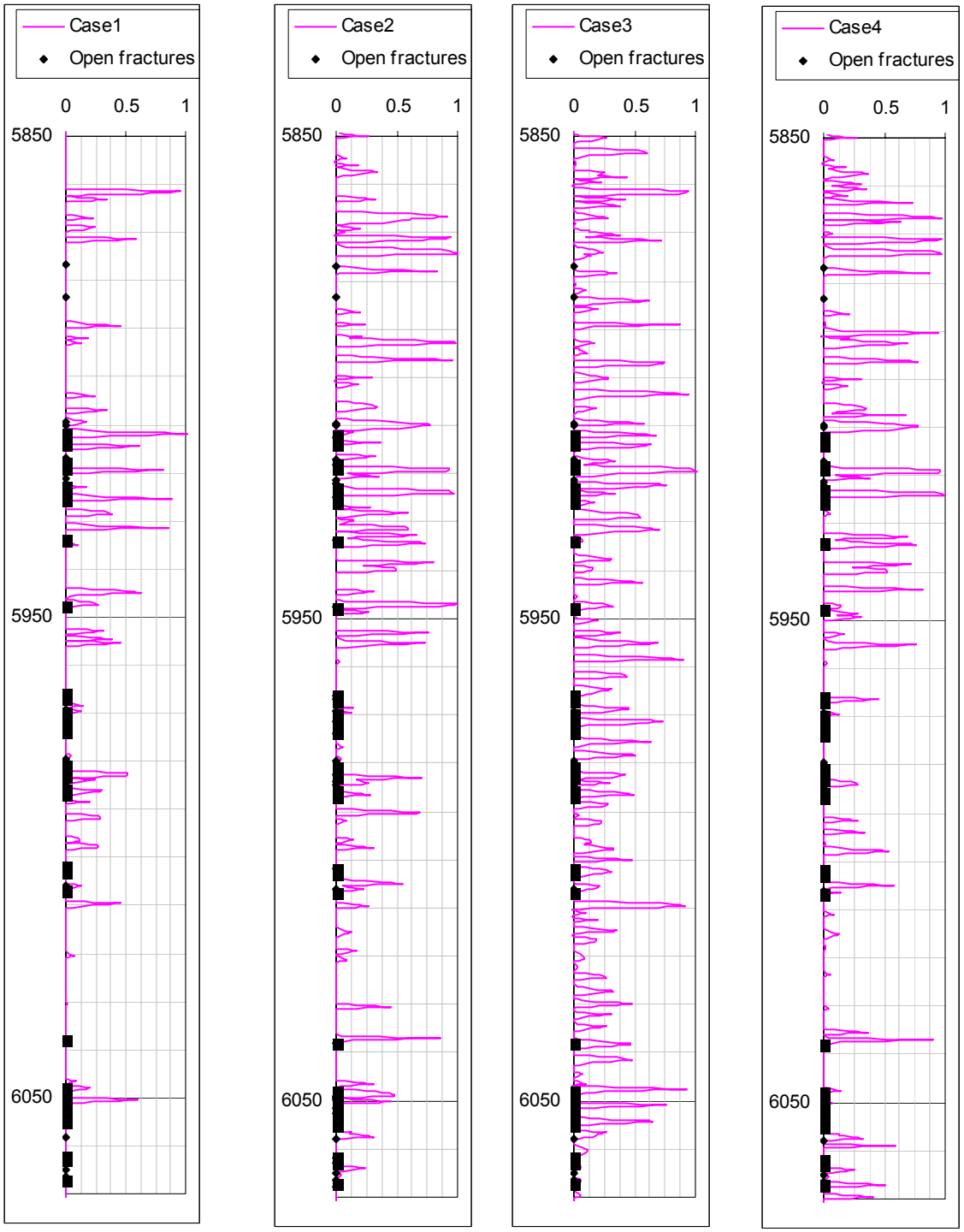

(a) **(b)** **(c)** **(d)**

Figure 22: Fuzzy Inference System Cases 1 – 4 (See Table 1 for Rules)

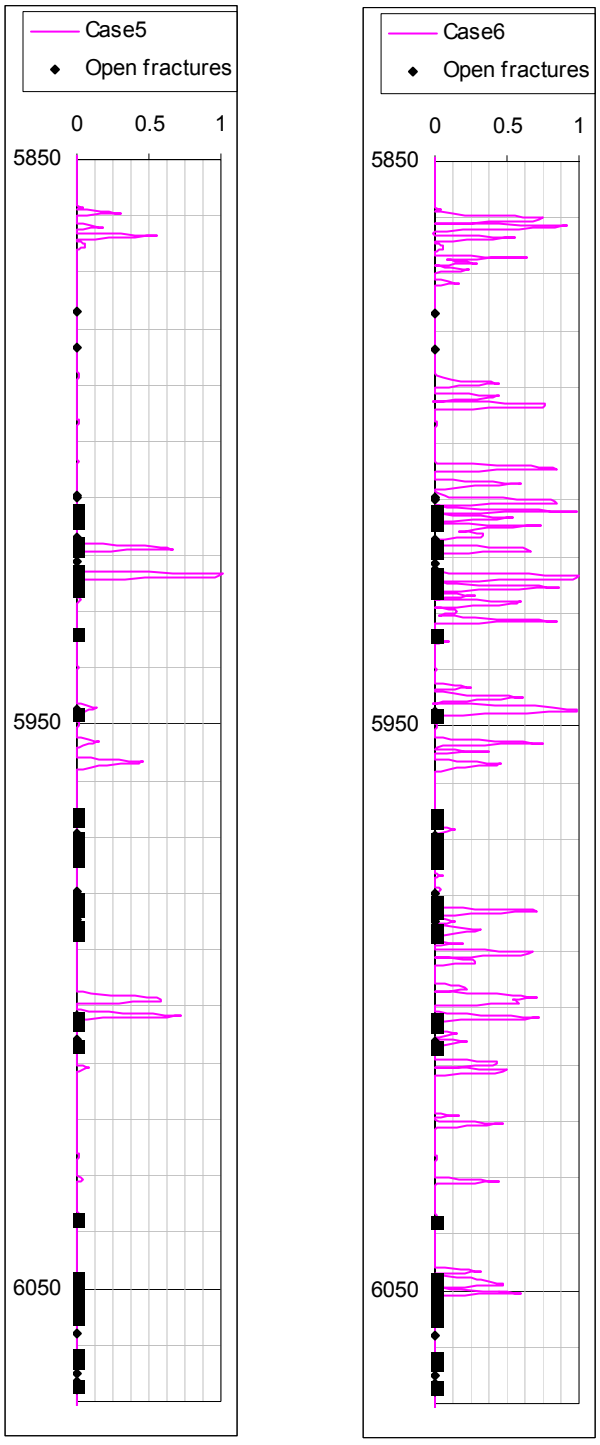

(a) **(b)**

Figure 23: Fuzzy Inference System Cases 5 and 6 (See Table 3 for Rules)

Table 3: Set of Rules used in the different cases for the FIS

CASE 1
IF SFL is high and AT10/AT90 is high **THEN** FI is high
IF DRHO is high and PEF is high **THEN** FI is high
CASE 2
IF DT is high and DRHO is high and CAL is high **THEN** FI is high
IF GR is high and SP is high and SFL is high **THEN** FI is high
IF DRHO is high and CAL is medium **THEN** FI is high
CASE 3
IF DT is high and SFL is high **THEN** FI is high
IF PEF is high and DRHO is high **THEN** FI is high
IF AT10/AT90 is high and ILD/ILM is high **THEN** FI is high
CASE 4
IF GR is high and PE **THEN** FI is high
IF DT is high and SFL high **THEN** FI is high
IF NPOR - DPHI is high and DRHO is high **THEN** FI is high
CASE 5
IF CAL is high and GR is high and SP is high **THEN** FI is high
IF DT is high and GR is high **THEN** FI is high
IF DT is high and SP is high **THEN** FI is high
CASE 6
IF CAL is high and GR is high and SP is high **THEN** FI is high
IF DT is high and GR is high **THEN** FI is high
IF DT is high and SP is high **THEN** FI is high
IF SFL is high and GR is high and SP is high **THEN** FI is high
IF SFL is high and AT10/AT90 is high **THEN** FI is high

The fractured interval reported by the core analysis between 5965 and 5975 ft is not recognized by any of the cases analyzed. This may indicate erroneous core description or, more likely a depth shift in the core analysis.

The high fracture frequency observed in zones where core analysis does not report fractures might indicate the presence of mechanically induced fractures that are excluded from the core description. However, the FIS algorithm may be responding to hairline fractures that are not accounted for in the core description provided.

Case 6 appears to be the most appropriate in this specific example. Case 6, uses the same rules as Case 5, but has two additional rules involving the resistivity and the SPF log. It is then

possible to conclude that induction and resistivity logs play a very important role in detecting fractures for this case.

The fracture porosity reported in Figure 24(c), clearly identifies several of the high fracture frequency zones reported by the core analysis, specifically the following intervals: 5920-5925 ft and 6000-6007 ft. However, there are zones where it is difficult to correlate the fracture porosity obtained with the O'Connell and Budiansky model and the one reported by the core analysis. The main reason that can explain this difficulty is the presence of more than 700 hairline fractures that are not classified as open or semi open fractures in the interval analyzed and may be affecting the fracture porosity results obtained. The whole interval reports a relatively high crack density and fracture porosity that may be reflecting the presence of a high number of hairline or mechanically induced fractures.

From Figure 24(d), it is possible to observe a fairly good correlation between the results obtained with the FIS and the inversion of O'Connell and Budiansky model in most of the intervals where the FIS reports a high fracture intensity index. This may lead us to the conclusion that the FIS system proposed might be used as fracture porosity indicator.

Discrepancies between core description of fractures and indicators of fractures using well logs are expected, due to a number of factors such as:

- Fracture indicators are based on well log data that reflect bulk rock properties up to several feet away from the borehole while the core analysis is only reflecting the characteristics of the borehole itself.

- In highly fractured zones it is difficult to obtain reliable core samples.

- Shifts between recorded core depths and well log depths (due to unfilled space in the core barrel, core expansion, stretch in the wireline logging cable, operator error, etc.).

Both models appear to be providing some information on the extent of fracturing, but it is unclear at this point how to quantify exactly what that information is. The next phase of the work will be to continue to find ways to use the two models to quantify both the accuracy and the uncertainty involved with using conventional well logs to estimate fracture properties. In addition, there is a need to be able to relate the information from these models and more sophisticated (Formation MicroScanner and Borehole Televiewer) log information to data collected at the surface- or crosswell-seismic scale. Also, work needs to be performed that relates this same information to flow properties for use in numerical simulation.

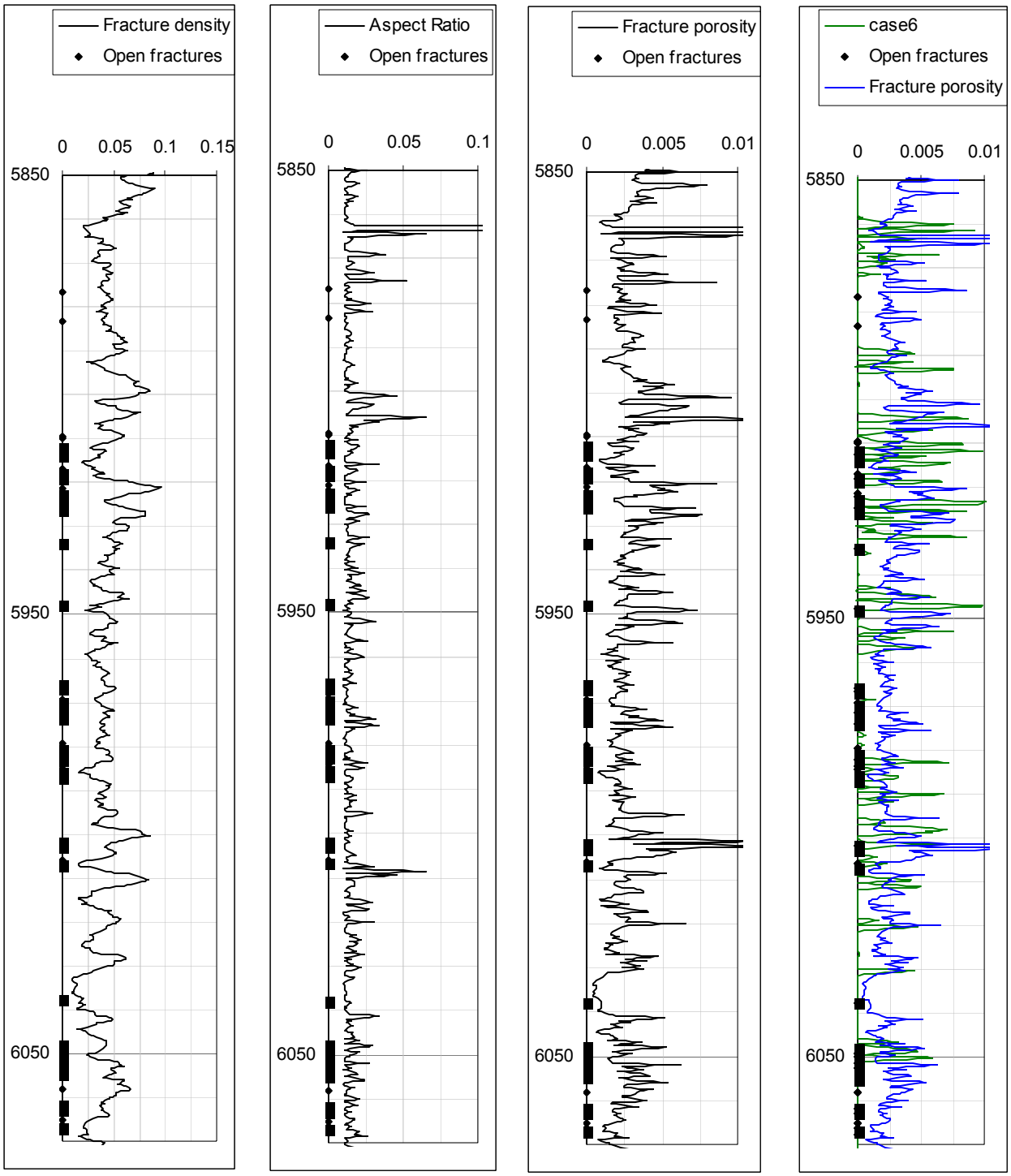

(a) **(b)** **(c)** **(d)**

Figure 24: O'Connell and Budiansky model results (a) Fracture Density, (b) Aspect Ratio, (c) Fracture Porosity and (d) Fracture Porosity with Fracture Index from FIS Case 6

Task III. Wellbore Models for Fractured Reservoir Systems

After a thorough literature review, it was decided to implement a wellbore system that assumes a horizontal wellbore open to flow along its total length and with a homogenous fluid flowing through it. Flow from both the fractures and matrix is allowed to occur and is considered through productivity indexes that are proportional to the equivalent fracture and matrix permeabilities, respectively. A similar approach has been implemented for the vertical well.

Wellbore hydraulics is taken into account by writing the flow equations in a form similar to the reservoir equations. The diffusivity equation that describes oil phase is given by

$$0.006328\ \frac{\partial}{\partial l}\left[\frac{k_p k_{rop}}{\mu_{op} B_{op}}\frac{\partial p_{wf}}{\partial l}\right] = -\frac{\partial}{\partial t}\left(\phi_p \frac{S_{op}}{B_{op}}\right) + 5.615\ Q_o - \left(q_o + q_{of}\right) \quad \text{.....68}$$

where l denotes the coordinate along the wellbore and p indicates that properties are evaluated at the conditions inside of the horizontal pipe, which in the case of PVT properties indicates they are evaluated at p_{wf}. For water, one has a similar equation

$$0.006328\ \frac{\partial}{\partial l}\left[\frac{k_p k_{rwp}}{\mu_{wp} B_{wp}}\frac{\partial p_{wf}}{\partial l}\right] = -\frac{\partial}{\partial t}\left(\phi_p \frac{S_{wp}}{B_{wp}}\right) + 5.615\ Q_w - \left(q_w + q_{wf}\right) \quad \text{.....69}$$

The following relationship can be written for the gas phase accounting for gas solubility in both the oil and water.

$$0.006328\ \frac{\partial}{\partial l}\left[k_p\left(\frac{k_{rgp}}{\mu_{gp} B_{gp}} + \frac{R_{sop} k_{rop}}{\mu_{op} B_{op}} + \frac{R_{swp} k_{rwp}}{\mu_{wp} B_{wp}}\right)\frac{\partial p_{wf}}{\partial l}\right]$$
$$= -\frac{\partial}{\partial t}\left[\phi_p\left(\frac{S_{gp}}{B_{gp}} + \frac{R_{sop} S_{op}}{B_{op}} + \frac{R_{swp} S_{wp}}{B_{wp}}\right)\right] + Q_g - \left(q_g + q_{gf}\right) \quad \text{.....70}$$

The "effective permeability in the pipe" is calculated from a mechanical energy balance where the kinetic and gravity effects are assumed negligible. After writing the homogenous fluid velocity in the wellbore in a form similar to the Darcy velocity of fluids through a porous media, the following expression is obtained for the effective permeability, k_p.

$$k_p = 9.2931 \times 10^9\ \phi_p \overline{\mu}\left[\frac{r_w}{\overline{\rho} f}\left|\frac{\partial p_{wf}}{\partial l}\right|^{-1}\right]^{\frac{1}{2}} \quad \text{.....71}$$

On the other hand, the pressure drop within the wellbore can be directly calculated from the mechanical energy balance according to the following equation.

$$\frac{\partial p_{wf}}{\partial l} = -2.8914 \times 10^{-14} \frac{f \bar{\rho} \bar{v}_p^2}{r_w} \quad \text{.....72}$$

By substituting Eq. 72 into Eq. 71, a more convenient expression for k_p is obtained.

$$k_p = 5.4652 \times 10^{15} \frac{\phi_p \bar{\mu} r_w}{\bar{\rho} f \bar{v}_p} \quad \text{.....73}$$

Several terms are involved in Eq. 73 and are explained in the following. The homogenous fluid properties are obtained as saturation weighted averages according to

$$\bar{\rho} = \rho_{op} S_{op} + \rho_{wp} S_{wp} + \rho_{gp} S_{gp} \quad \text{.....74}$$

$$\bar{\mu} = \mu_{op} S_{op} + \mu_{wp} S_{wp} + \mu_{gp} S_{gp} \quad \text{.....75}$$

The assumption of homogenous fluid is good as long as density and viscosity of phases can be represented by the average mixture properties.

The "equivalent wellbore porosity" is calculated as the ratio of the wellbore volume to the total grid-block (bulk) volume, V.

$$\phi_p = \frac{\pi r_w^2 \Delta l}{V} \quad \text{.....76}$$

The traditional Fanning friction factor, f, is also required in Eq. 73. For laminar flow ($N_{Re} <$ 2100), the friction factor is a function of the Reynolds number according to the following relation.

$$f = \frac{16}{N_{Re}} \quad \text{.....77}$$

For turbulent flow, the friction factor depends on the roughness of the pipe and the Reynolds number. Among several correlations available in the literature, Aziz et al. recommended the equation proposed by Colebrook

$$\frac{1}{\sqrt{f}} = 4 \log\left(\frac{r_w}{e}\right) + 3.48 - 4 \log\left(1 + 9.35 \frac{r_w}{e N_{Re} \sqrt{f}}\right) \quad \text{.....78}$$

The actual in-situ velocity, v_p, is calculated by dividing the Darcy velocity by the equivalent wellbore porosity

$$\bar{v}_p = -0.006328 \frac{k_p}{\phi_p \bar{\mu}} \frac{\partial p_{wf}}{\partial l} \quad \text{.....79}$$

The solution of Eq. 73 requires an implicit evaluation. Sharma et al. suggested an explicit evaluation using the average in-situ velocity given by Eq. 79. They pointed out that this is a good approximation since pressure gradients and fluid properties do not significantly change between time steps under pseudo-steady-state wellbore flow conditions.

In Eqs. 68-70, linear relative permeability curves are assumed for homogenous flow according to

$$k_{rop} = S_{op} \quad \text{.....80}$$

$$k_{rgp} = S_{gp} \quad \text{.....81}$$

$$k_{rwp} = S_{wp} \quad \text{.....82}$$

The boundary conditions connect the wellbore model with the reservoir model. The fluid transfer term between the matrix and the wellbore is defined as follows.

$$q_i = \tilde{q}_i \, V \qquad i = o, w, g \quad \text{.....83}$$

where $\tilde{q}_i$ is the flow rate per unit volume of the phase *i* used as source/sink term in Eqs. 90-92 and *V* is the grid-block volume. Similar expression can be written for the fluid transfer between the fractures and the wellbore.

Peaceman's approximation was implemented to calculate flow rates from the matrix into the wellbore. For the oil phase, the rate is from the matrix to the wellbore is calculated by

$$q_o = I\left(\frac{k_{ro}}{\mu_o B_o}\right)\left(p_I - p_{wf}\right) \quad \text{.....84}$$

while the following equation is used to calculate the rate from the fracture to the wellbore.

$$q_{of} = I_f\left(\frac{k_{rof}}{\mu_{of} B_{of}}\right)\left(p_f - p_{wf}\right) \quad \text{.....85}$$

where the well indexes, I, are calculated from

$$I = 0.00708 \frac{k_m \, \Delta l}{ln\left(\frac{r_o}{r_w}\right) + s} \quad \text{.....86}$$

The radius r_o may be estimated from the Peaceman's formula

$$r_o = 0.28 \frac{\left[\left(\frac{k_z}{k_y}\right)^{1/2} \Delta y^2 + \left(\frac{k_y}{k_z}\right)^{1/2} \Delta z^2\right]^{1/2}}{\left(\frac{k_z}{k_y}\right)^{1/4} + \left(\frac{k_y}{k_z}\right)^{1/4}} \quad \text{.....87}$$

The fracture index, I_f, requires fracture characteristics such the permeability scalar in the grid block and fracture half length to calculate the appropriate value.

$$I_f = 0.00708 \frac{\left|k_f\right| \Delta l}{ln\left(\frac{L_f}{r_w}\right) + s_f} \quad \text{.....88}$$

On the other hand, Q_i correspond to the imposed injection/production rates from/into the horizontal well. Finally, an auxiliary equation describing the volumetric balance within the horizontal pipe is required.

$$S_{gp} + S_{op} + S_{wp} = 1 \quad \text{.....89}$$

The previous formulation was coded into the naturally fractured simulator.

Task IV. Reservoir Simulator Development

Modifications to a generalized naturally fractured reservoir simulator developed by Ohen and Evans (1990) based on work proposed by Evans (1982) serve as the basis of the naturally fractured reservoir simulator. The simulator is a three-dimensional, three-phase black oil simulator developed to describe fluid flow in a naturally fractured reservoir based on the BOAST formulation. The program was developed for use in a desktop personal computer environment.

The resulting relations for flow of oil, water, and gas through the matrix are as follows:

$$0.006328\,\nabla\left[\frac{\overline{\overline{k_l}}k_{ro}}{\mu_o B_o}\left(\Delta p_l-\frac{\rho_o}{144}\Delta D\right)\right]=-\frac{\partial}{\partial t}\left(\phi_l\frac{S_o}{B_o}\right)-\tilde{q}_o-\Gamma_o \quad \text{.....90}$$

$$0.006328\,\nabla\left[\frac{\overline{\overline{k_l}}k_{rw}}{\mu_w B_w}\left(\Delta p_l-\Delta P_{cwol}-\frac{\rho_w}{144}\Delta D\right)\right]=-\frac{\partial}{\partial t}\left(\phi_l\frac{S_w}{B_w}\right)-\tilde{q}_w-\Gamma_w \quad \text{.....91}$$

$$0.006328\,\nabla\left[\begin{array}{l}\frac{\overline{\overline{k_l}}k_{rg}}{\mu_g B_g}\left(\Delta p_l+\Delta P_{cgol}-\frac{\rho_g}{144}\Delta D\right)+\\ R_{so}\frac{\overline{\overline{k_l}}k_{ro}}{\mu_o B_o}\left(\Delta p_l-\frac{\rho_o}{144}\Delta D\right)+\\ R_{sw}\frac{\overline{\overline{k_l}}k_{rw}}{\mu_w B_w}\left(\Delta p_l-\Delta P_{cwol}-\frac{\rho_w}{144}\Delta D\right)\end{array}\right]$$
$$=-\frac{\partial}{\partial t}\left[\phi_l\left(\frac{S_g}{B_g}+R_{so}\frac{S_o}{B_o}+R_{sw}\frac{S_w}{B_w}\right)\right]-\tilde{q}_g-\Gamma_g \quad \text{.....92}$$

The matrix permeability is a zero-nondiagonal tensor given by

$$\overline{\overline{k_l}}=\begin{bmatrix}k_x & 0 & 0\\ 0 & k_y & 0\\ 0 & 0 & k_z\end{bmatrix} \quad \text{.....93}$$

The fluid interaction term that takes into account the mass transfer from the primary rock matrix into the fractures per unit time per unit volume of the medium is described by the following steady-state approximations for oil, water, and gas.

$$\Gamma_o=C\frac{k_{ro}}{\mu_o B_o}\left(p_l-p_f\right) \quad \text{.....94}$$

$$\Gamma_w=C\frac{k_{rw}}{\mu_w B_w}\left(p_l-p_f-P_{cowl}+P_{cowf}\right) \quad \text{.....95}$$

$$\Gamma_o = C\left[\begin{array}{l}\dfrac{k_{rg}}{\mu_g B_g}\left(p_1 - p_f + P_{cgo1} - P_{cgof}\right) + \dfrac{R_{so}k_{ro}}{\mu_o B_o}\left(p_1 - p_f\right) \\ + \dfrac{R_{sw}k_{rw}}{\mu_w B_w}\left(p_1 - p_f - P_{cow1} + P_{cowf}\right)\end{array}\right] \quad \text{.....96}$$

In Eqs. 94-96, the fluid transfer constant, C, is given by

$$C = 0.006328\ \frac{k_m \phi_f}{r_H L_f} \quad \text{.....97}$$

where k_m is an average matrix permeability obtained from Eq. 93.

The fractured system is modeled as an anisotropic media in which fluids flow according to Darcy's law. In the original model proposed by Evans (1982) an additional acceleration term was included in the equations of motion. However, numerical experiments indicate that the acceleration term contributes with a negligible pressure drop along the fracture. The diffusivity equation that describes the flow through the fractures for oil, water, and gas are as follows.

$$0.006328\ \nabla\left[\frac{\overline{\overline{k_f}}k_{rof}}{\mu_{of}B_{of}}\left(\Delta p_f - \frac{\rho_{of}}{144}\Delta D\right)\right] = -\frac{\partial}{\partial t}\left(\phi_f \frac{S_{of}}{B_{of}}\right) - \tilde{q}_{of} + \Gamma_o \quad \text{.....98}$$

$$0.006328\ \nabla\left[\frac{\overline{\overline{k_f}}k_{rwf}}{\mu_{wf}B_{wf}}\left(\Delta p_f - \Delta P_{cwof} - \frac{\rho_{wf}}{144}\Delta D\right)\right] = -\frac{\partial}{\partial t}\left(\phi_f \frac{S_{wf}}{B_{wf}}\right) - \tilde{q}_{wf} + \Gamma_w \quad \text{.....99}$$

$$0.006328\ \nabla\left[\begin{array}{l}\dfrac{\overline{\overline{k_f}}k_{rgf}}{\mu_{gf}B_{gf}}\left(\Delta p_f + \Delta P_{cgof} - \dfrac{\rho_{gf}}{144}\Delta D\right) + \\ R_{sof}\dfrac{\overline{\overline{k_f}}k_{rof}}{\mu_{of}B_{of}}\left(\Delta p_f - \dfrac{\rho_{of}}{144}\Delta D\right) + \\ R_{swf}\dfrac{\overline{\overline{k_f}}k_{rwf}}{\mu_{wf}B_{wf}}\left(\Delta p_f - \Delta P_{cwof} - \dfrac{\rho_{wf}}{144}\Delta D\right)\end{array}\right]$$
$$= -\frac{\partial}{\partial t}\left[\phi_f\left(\frac{S_{gf}}{B_{gf}} + R_{sof}\frac{S_{of}}{B_{of}} + R_{swf}\frac{S_{wf}}{B_{wf}}\right)\right] - \tilde{q}_{gf} + \Gamma_g \quad \text{.....100}$$

The fracture permeability is modeled as a nondiagonal tensor given by

$$\overline{\overline{k}}_f = \begin{bmatrix} k_{xx} & k_{xy} & k_{xz} \\ k_{yx} & k_{yy} & k_{yz} \\ k_{zx} & k_{zy} & k_{zz} \end{bmatrix} \quad \text{.....101}$$

Avila *et al.* (2000) showed that Eq. 101 can be written in a more convenient form. They stated that the fracture permeability tensor can be obtained as a product of two independent functions

$$\overline{\overline{k}}_f = |k_f| \left[\overline{\overline{k}}_f \right] \quad \text{.....102}$$

The unit permeability tensor, $\left[\overline{\overline{k}}_f\right]$, is calculated at specific points in the reservoir where the orientation of the fractures are known. After interpolating/extrapolating fracture orientation in the reservoir domain, the permeability tensor is obtained by multiplying the unit permeability tensor by the permeability scalar, $|k_f|$. In regions of the reservoir where no fractures are present the model exhibits a numerical instability that is overcome by multiplying the unit permeability by the average matrix permeability, k_m.

Auxiliary equations are required to solve this system of equations include the requirement that the saturations in the matrix and the fractures must equal one.

$$S_g + S_o + S_w = 1 \quad \text{.....103}$$

$$S_{gf} + S_{of} + S_{wf} = 1 \quad \text{.....104}$$

In addition, independent capillary pressure relationships for the matrix and the fractures are required as functions of saturation.

$$P_{cow1} = p_1 - p_w = f(S_w) \quad \text{.....105}$$

$$P_{cgo1} = p_g - p_1 = f(S_g) \quad \text{.....106}$$

$$P_{cowf} = p_f - p_{wf} = f(S_{wf}) \quad \text{.....107}$$

$$P_{cgof} = p_{gf} - p_f = f(S_{gf}) \quad \text{.....108}$$

In the general case, the reservoir is modeled as a rectangular parallelepiped with an external no-flow boundary but a constant potential boundary can be easily implemented. The

inner boundary condition is either constant rate or pressure as described in the formulation of the wellbore system. The previous partial differential equations were solved using a finite difference formulation and IMPES solution scheme.

In developing the fractured reservoir simulator, the BOAST-VHS code was translated from FORTRAN to Visual Basic and implemented with macros in an Excel-VB environment. This translation was undertaken to assist in providing a PC-based simulator that can be easily implemented without a major investment in computer hardware or software. The ability to use a simple spreadsheet application for data input and output will allow the user the ability to use the graphics capability of the spreadsheet software for visualizing the results, eliminating the need for a sophisticated graphics package.

The simulator was modified to incorporate Evan's naturally fractured reservoir model, the fracture permeability tensor, and the developed wellbore models. The resulting simulator was named BOAST-NFR to reflect the original source code and the NFR representing naturally fractured reservoir. The new simulator was tested for both single-phase and two-phase flow for single-porosity systems and yielded the appropriate solutions. The developed simulator uses an IMPES solution to the linear equations. The simultaneous solution of the pressure equations for the fracture and matrix is handled using LSOR.

The naturally fractured simulator has the following characteristics.

1. Numerical simulation of oil and/or gas recovery by fluid expansion, displacement, gravity drainage, and imbibition mechanisms.
2. Rectangular grid-blocks with variable dimensions.
3. Zero transmissibility option (inactive grid blocks).
4. Simulation of tilted reservoirs by specifying the elevations to top of grid-blocks.
5. Porosity and permeability distributions for matrix and fracture systems. For fracture permeability, the model requires a diagonal tensor.
6. Different relative permeability and capillary pressure tables for matrix and fracture systems.
7. Pore matrix and fracture compressibility table.
8. Oil-water-gas PVT tables for reservoir fluids.
9. Bubble point pressure tracking scheme.
10. Pressure and saturation initialization for both porous media.
11. Automatic time-step control.
12. Option for automatic control of LSOR acceleration parameter.
13. Material balance check on solution stability.
14. Vertical and horizontal wells with specification of rate or pressure constraints on well performance.
15. Capabilities to add wells during the time period represented by the simulation.

Penuela (2002) provides additional details regarding the development of the simulator. BOAST-NFR and the BOAST-NFR Users Guide are provided as a stand-alone document furnished to the United States Department of Energy.

Task V. Technology Transfer

The technology transfer aspect of this project has been accomplished through technical paper publication, technical conference presentations, and workshops. Two workshops were held during the course of this project in Norman (December 2000) and Oklahoma City (March 2001). The 2000 workshop included twenty-seven participants and provided attendees with an overview of the research project and the current status of activities. The 2001 workshop was conducted in cooperation with the Oklahoma City Section of the Society of Petroleum Engineer during the Production and Operations Symposium. Over this two-day conference, the project team made six technical presentations, with an average attendance of 46 attendees.

In June 2002, the University of Oklahoma hosted a two-day conference on naturally fractured reservoirs. The Conference on Naturally Fractured Reservoirs was held on 3-4 June 2002 in Oklahoma City and was organized by the Mewbourne School of Petroleum and Geological Engineering and the Oklahoma Geological Survey. Abstracts were solicited from industry, research, and academic groups with an interest in naturally fractured reservoirs to develop the technical program. The technical program had seventeen presentations and these technical papers were published in a CD-rom proceedings volume that was distributed to the participants. The conference was attended by 94 participants from eight US states and Canada. Those registered for the conference represented industry, government, and academia. The conference was sponsored by Anadarko Petroleum, Devon Energy, EOG Resources, Kerr-McGee, Marathon Oil, and Phillips Petroleum. A copy of the Proceedings will be submitted with this report.

Papers Presented at the Conference Naturally Fractured Reservoirs:

NFR-001 **The Origin of Natural Fracturing**, S.P. Gay, Jr., Applied Geophysics, Inc.

NFR-002 **Evaluation of Fracture Mechanisms for the Spraberry Trend, Midland Basin**, B.J. McPherson and D.F. Boutt, New Mexico Institute of Mining and Technology

NFR-003 **Elongated Slab Models for Interporosity Flow in Naturally Fractured Reservoirs**, G. Penuela, R.G. Hughes, F. Civan and M.L. Wiggins, U. of Oklahoma

NFR-004 **Modeling Coupled Fracture-Matrix Fluid Flow in Geomechanically Simulated Fracture Networks**, Z.G. Philip, J.W. Jennings, Jr., J.E. Olson, J. Holder, U. of Texas at Austin

NFR-005 **Investigating the Sensitivity of Input Data on the Quality of Fracture Network Realizations**, J.M. Herrin and L. Teufel, New Mexico Institute of Mining and Technology

NFR-006 **Integrating NMR, Neutron-Density, and Resistivity Logs to Detect Natural Fractures**, W. Thungsuntonkhun and T.W. Engler, New Mexico Institute of Mining and Technology

NFR-007 **Transcending Conventional Log Interpretation – A More Effective Approach for the Spraberry Trend Area**, D. Alfred, E. Putra and D.S. Schechter, Texas A&M U.

NFR-008 **Fractured Reservoir Properties from Conventional Well Logs**, L. Martinez and R.G. Hughes, U. of Oklahoma

NFR-009 **A General Model for Fracture Compliance and Permeability**, R.L. Brown, Oklahoma Geological Survey

NFR-010 **Integration of 3-D Seismic, Well Test and Core Data to Simulate Permeability**

Descriptions, A. Bahar and H. Ates, Kelkar and Associates, Inc., and M. Kelkar, U. of Tulsa

NFR-011 **Advantages and Limitations of Different Methods for Assessing Natural Fractures in the Raton Bason of Colorado and New Mexico**, C.A. Rautman, S.P. Cooper and B.W. Arnold, Sandia National Laboratories, P.M. Basinski, El Paso Production Co., T.H. Mroz, National Technology Energy Laboratory, and J.C. Lorenz, Sandia National Laboratories

NFR-012 **Frequency Dependence of Fractured Reservoirs**, E.M. Chesnokov, U. of Oklahoma and R.L. Brown, Oklahoma Geological Survey

NFR-013 **Improving Dual-Porosity Simulation in the Naturally Fractured Spraberry Trend Area**, T. Chowdhury, G. Dabiri, E. Putra and D.S. Schechter, Texas A&M U.

NFR-014 **Reservoir Characteristics of Fractured Reservoirs of the Monterey Formation**, I. Ershaghi, U. of Southern California, S. Horner and K. Christensen, Venoco, Inc.

NFR-015 **Waterflood Performance in the Naturally Fractured Spraberry Trend Area, West Texas**, D.S. Schechter and E. Putra, Texas A&M U., R.O. Baker, Epic Consulting Services, Ltd., W.H. Knight, W.P. McDonald, P. Leonard and C. Rounding, Pioneer Natural Resources, USA

NFR-016 **Characterization and Fluid-Flow Stimulation of Naturally Fractured Tight-Gas Sandstone Reservoirs**, L.W. Teufel, New Mexico Institute of Mining and Technology

NFR-017 **Integrated Modeling of Flow in Naturally Fractured Reservoirs**, R.G. Hughes, L. Martinez, G. Penuela, F. Civan and M.L. Wiggins, U. of Oklahoma and R.L. Brown, Oklahoma Geological Survey

Technical Presentations or Publications by the Research Team:

Wiggins, M.L.: "Status of the Naturally Fractured Reservoir Characterization Project," presentation at the US DOE, NPTO's Program Review, Denver, CO, June 26-29, 2000.

Avila, R.E., Gupta, A., Penuela, G.: "An Integrated Approach to the Determination of Permeability Tensors in Naturally Fractured Reservoirs," International Petroleum Conference 2000, Calgary, June 4-8, 2000.

Brown, R.L., Wiggins, M.L., and Gupta, A.: "Fracture Roughness: The Key to Relating Seismic Velocities, Seismic Attenuation and Permeability to Reservoir Pressure and Saturation," SEG Annual Meeting and International Exposition, Calgary, August 6-11, 2000.

Brown, R.L., Wiggins, M.L. and Gupta, A.: "Seismic Determination of Saturation in Fractured Reservoirs," paper SPE 67278 presented at the 2001 SPE Production and Operations Symposium, Oklahoma City, OK, March 25-28.

Civan, F. and Rasmussen, M.L.: "Improved Prediction of Waterflood Sweep Efficiency Using Multiexponent Matrix-to-Fracture Transfer Functions," paper SPE 67279 presented at the 2001 SPE Production and Operations Symposium, Oklahoma City, OK, March 25-28.

Martinez, L.P. and Gupta, A.: "Interpretation of Important Fracture Characteristics From Conventional Well Logs," paper SPE 67280 presented at the 2001 SPE Production and Operations Symposium, Oklahoma City, OK, March 25-28.

Gupta, A.: "Characterization of Mass Transfer from Matrix to Fractures," paper SPE 67282 presented at the 2001 SPE Production and Operations Symposium, Oklahoma City, OK, March 25-28.

Quintero, E.J., Martinez, L.P. and Gupta, A.: "Characterization of Naturally Fractured Reservoirs Using Artificial Intelligence," paper SPE 67286 presented at the 2001 SPE Production and Operations Symposium, Oklahoma City, OK, March 25-28.

Brown, R.L., Gutpa, A. and Wiggins, M.L.: "Problems Calibrating Production and Seismic Data for Fractured Reservoirs," paper SPE 67317 presented at the 2001 SPE Production and Operations Symposium, Oklahoma City, OK, March 25-28.

Brown, R.L., Parra, J.O. and Xu, P.C.: "Seismic Attenuation and Flow Properties in Fractured Reservoirs," Seventy-First Annual Meeting, SEG International Exposition, Calgary, Expanded Abstracts, 1678-1681.

Chen, H., Brown, R.L., and Castanga, J.P.: "Synthetic Multicomponent AVO Study of Fractured Reservoir Models with Multiple Fracture Sets," presented at the SEG Meeting, San Antonio, TX, October 2001.

Chen, H., Castanga, J.P., Brown, R.L., and Ramos, A.C.B.: "Three-Parameter AVO Crossplotting in Anistropic Media," Geophysics, 66, 1359-1363.

Penuela,G., Hughes, R.G., Civan, F. and Wiggins, M.L.: "Time-Dependent Shape Factors for Secondary Recovery in Naturally Fractured Reservoirs," paper SPE 75234 presented at the SPE/DOE 13th Symposium on Improved Oil Recovery, Tulsa, OK, April 13-17, 2002.

Penuela, G., Civan, F., Hughes, R.G. and Wiggins, M.L.: "Time-Dependent Shape Factors for Interporosity Flow in Naturally Fractured Gas Condensate Reservoirs," paper SPE 75524 presented at the 2002 SPE Gas Technology Symposium, Calgary, Alberta, Canada, April 30 – May 2, 2002.

Penuela, G., Civan, F., Hughes, R.G. and Wiggins, M.L.: "Models for Interporosity Flow in Naturally Fractured Reservoirs," paper NFR-002 presented at the OU Conference on Naturally Fractured Reservoirs, Oklahoma City, OK, June 3-4, 2002.

Martinez, L. and Hughes, R.G.: "Fractured Reservoir Properties from Conventional Well Logs," paper NFR-008 presented at the OU Conference on Naturally Fractured Reservoirs, Oklahoma City, OK, June 3-4, 2002.

Brown, R.L.: “A General Model for Fracture Compliance and Permeability,” paper NFR-009 presented at the OU Conference on Naturally Fractured Reservoirs, Oklahoma City, OK, June 3-4, 2002.

Chesnokov,E.M. and Brown, R.L.: “Frequency Dependence of Fractured Reservoirs,” paper NFR-012 presented at the OU Conference on Naturally Fractured Reservoirs, Oklahoma City, OK, June 3-4, 2002.

Brown, R.L., Wiggins, M.L. and Gupta, A.: “Seismic Determination of Saturation in Fractured Reservoirs,” *SPE Journal* (September 2002) 237-242.

Conclusion

This research project has focused on estimating naturally fractured reservoir properties from seismic data, predicting fracture characteristics from well logs, and developing a naturally fractured reservoir simulator. It is important to develop techniques that can be applied to estimate the important parameters in predicting the performance of naturally fractured reservoirs as many oil and gas reservoirs in the United States are naturally fractured. It is estimated that from 70-90% of the original oil and gas in place in such complex reservoir systems are still available for recovery, provided new technology can be implemented to exploit these reservoirs in an efficient and cost effective manner.

This project was focused on developing a systematic reservoir characterization methodology which can be used by the petroleum industry to implement infill drilling programs and/or enhanced oil recovery projects in naturally fractured reservoir systems in an environmentally safe and cost effective manner. This research program has been guided to provide geoscientists and engineers with techniques and procedures for characterizing a naturally fractured reservoir system and developing a desktop naturally fractured reservoir simulator.

This project proposes a method to relate seismic properties to the elastic compliance and permeability of the reservoir based upon a sugar cube model. In addition, methods are presented to use conventional well logs to estimate localized fracture information for reservoir characterization purposes. The ability to estimate fracture information from conventional well logs is very important in older wells where data are often limited. Finally, a desktop naturally fractured reservoir simulator has been developed for the purpose of predicting the performance of these complex reservoirs. The simulator incorporates vertical and horizontal wellbore models, methods to handle matrix to fracture fluid transfer, and fracture permeability tensors.

The ability to obtain naturally fractured reservoir parameters from seismic data, well logs, and engineering data is an important component to simulating these reservoirs. With the proper fracture properties, the naturally fractured reservoir simulator can be used to select well locations and evaluate exploitation strategies to optimize the recovery of the oil and gas reserves from such complex reservoir systems.

The project researchers organized a Conference on Naturally Fractured Reservoirs that was held in June 2002 and attracted over 90 participants. This symposium served as the major technology transfer activity for the project. The conference was very well received by both industry and academia and was a successful venue for the sharing of information related to exploiting naturally fractured reservoirs.

This research project has developed methods to characterize and study the performance of naturally fractured reservoirs that integrate geoscience and engineering data. This is an important step in developing exploitation strategies for optimizing the recovery from naturally fractured reservoir systems. The next logical extension of this work is to apply the proposed methods to an actual field case study to provide information for verification and modification of the techniques and simulator.

References

Avila, R., Gupta, A., and Peneula, G., 2000: "An Integrated Approach to the Determination of Permeability Tensors for Naturally Fractured Reservoirs," paper 2000-47 presented at the Canadian International Petroleum Conference, Calgary, June 4-8.

Bassiouni, Z., 1994: *Theory, Measurement, and Interpretation of Well Logs*, Society of Petroleum Engineers, SPE Textbook Series Vol. 4.

Brown, R.J.S. and Korringa, J., 1975: "On the Dependence of the Elastic Properties of a Porous Rock on the Compressibility of the Pore Fluid," Geophysics 40, 606-616.

Brown, R.L., Gupta, A., Wiggins, M.L., 2001, "Problems Calibrating Production and Seismic Data for Fractured Reservoirs," paper SPE 67317 presented at the SPE Production and Operations Symposium, Oklahoma City, OK, March 25-28.

Brown, R.L., Parra, J.O., Xu, P.C., 2001, Seismic Attenuation and Flow Properties in Fractured Reservoirs," Expanded Abstracts, 2001 SEG International Mtg., San Antonio.

Brown, R.L., Penuela, G., Hughes, R.G., Wiggins, M.L., and Civan, F., Martinez Torres, L., 2002a: "A Sugar Cube Model for the Elastic Compliance and Permeability of Reservoirs with Multiple Fracture Sets," submitted to Geophysics (SEG).

Brown, R.L., Wiggins, M.L., Penuela, G., Gupta, A. and Evans, R., 2002b: "Using Fracture Aperture to Relate the Permeability and Elastic Properties of Fractured Reservoirs," submitted to Geophysics (SEG).

Brown, R.L., Wiggins, M.L. and Gupta, A., 2002c: "Seismic Determination of Saturation in Fractured Reservoirs," SPEJ, September, 237-242.

Brown, R.L., Wiggins, M.L. Penuela, G., Hughes, R.G., Civan, F., and Martinez Torres, L., 2002d: "Using Saturation and Permeability Measurements to Constrain The Elastic Properties of Fractured Rocks," submitted to Geophysics (SEG).

Brown, R.L., Wiggins, M.L., Penuela, G., Hughes, R.G., Civan, F., and Martinez Torres, L., 2002e, "An Interpretation of Unexpected P- and S- Wave Responses Observed Over a Fractured Carbonate," submitted to Geophysics (SEG).

Brown, S.R., and Bruhn, R.L., 1998: Fluid Permeability of Deformable Fracture Networks," J. of Geophys. Res., 103 (B2), 2489-2500.

Chang, M-M. et. al., 1992: "Users Guide and Documentation Manual for BOAST-VHS for the PC," final report, Contract No. DE-FC22-83FE60149, U.S. DOE, Bartlesville, OK.

Crary, S. et al. 1987: "Fracture Detection With Logs," The Technical Review, V. 35, No. 1, 23-34.

Cox, E., 1994: *The Fuzzy Systems Handbook*, Academic Press.

Evans, R.D., 1982: "A Proposed Model for Multiphase Flow Through Naturally Fractured Reservoirs," *SPEJ* (Oct. 1982) 669-80.

Fertl, W. H., 1980: "Evaluation of Fractured Reservoirs Using Geophysical Well Logs," SPE paper 8938 presented at the 1980 SPE/DOE Symposium on Unconventional Gas Recovery held in Pittsburgh, Pensilvania, May 18-21, 1980.

Gassmann, F., 1951: "Uber die Elasticitat poroser Medien," Vierteljahrschrift der Naturforschenden Gessellschaft in Zurich, 96, 1-23.

Goldenberg, I. and Gurevich, B., 1998: "A Semi-Empirical Velocity-Porosity-Clay Model For Petrophysical Interpretation Of P- And S- Velocities," Geophysical Prospecting, 46, 217-285.

Greenberg, M.L., and Castagna, J.P., 1992: "Shear Wave Velocity Estimation In Porous Rocks: Theoretical Formulation, Preliminary Verification And Application," Geophysical Prospecting, 40, 195-209.

Guest, S., van der Kolk, C., Potters, H.: "The Effect of Fracture Filling Fluids on Shear-Wave Propagation," 68th Ann. International Mtg., SEG, Expanded Abstracts, 948-951.

Klir, G.J. and Yuan, B., 1995: *Fuzzy Sets and Fuzzy Logic, Theory and Applications*. Prentice Hall.

Lee, C.C., 1990: *Fuzzy Logic in Control Systems: Fuzzy Logic Controller*, Part II. IEEE Transactions on Systems, Man and Cybernetics, 20(2):419-435.

Lorenz, J., 1997: Sandia National Labs Internal Memo, August 18, 1997.

Martinez, L.P., Gupta, A. and Brown, R.L., 2001: "Interpretation of Important Fracture Characteristics From Conventional Well Logs," paper SPE 67280 presented at the 2001 SPE Production Operations Symposium, Oklahoma City, OK, March 24-27.

Mathworks, 1999: *Signal Processing Toolbox User's Guide*, The Mathworks Inc.

Mathworks, 1999: *Fuzzy Logic Toolbox User's Guide*. The Mathworks Inc.

Mavko, G., Mukerji, T., and Dvorkin, J., 1998: *The Rock Physics Handbook: Tools For Seismic Analysis In Porous Media*, Cambridge University Press.

Nauck, D., Klawonn, F., and Kruse, R., 1997: *Foundations of Neuro-Fuzzy Systems*, John Wiley & Sons, UK.

O'Connell, R.J., 1984: "A Viscoelastic Model of Anelasticity of Fluid Saturated Porous Rocks," Physics and Chemistry of Porous Media, AIP Conf. Proceedings, p.166-175.

Oda, M., 1985: "Permeability Tensor for Discontinuous Rock Masses," Geotechnique, 35, 483-495.

Ohen, H. and Evans, R.D., 1990: "Improved Simulation of Gas/Oil Drainage and Water/Oil Imbibition in a Naturally Fractured Reservoir," Report to the National Institute for Petroleum and Energy Research, Contract 160421.

Penuela, G., 2002: "Modeling Interporosity Flow for Improved Simulation of Naturally Fractured Reservoirs," Ph.D. Thesis, U. of Oklahoma, Norman, OK.

Rasolofosaon, P.N.J. and Zinszer, B.E., 2002: "Comparison Between Permeability Anisotropy and Elasticity Anistropy of Reservoir Rocks," Geophysics, 67, 230-240.

Rider, M.H. 1986: *The Geological Interpretation of Well Logs*. Blackie Halsted Press.

Roger, J.S., Sun, C.T., Mizutani, E., 1997: *Neuro-Fuzzy and Soft Computing*. Prentice Hall, Upper Saddle River, NJ.

Schlumberger, 1989: *Log Interpretation Principles/Applications*, Schlumberger Educational Services, Houston TX.

Schoenberg, M. and Sayers, C.M., 1995: "Seismic Anisotropy of Fractured Rock," Geophysics 60, 204-211.

Serra, O., 1986: *Fundamentals of Well Log Interpretation*, Elsevier Science Publishers B.V.

Sharma, R., Zimmerman, D., and Mourits, F., 1995: "Modeling of Undulating Wellbore Trajectories," J. of Canadian Petroleum Technology, Dec. 1995, 16-24.

Suau, J. and Gartner, J., 1980: "Fracture Detection From Well Logs," The Log Analyst. March-April, 3-13.

Xu, S., and White, R.E., 1996: "A Physical Model For Shear-Wave Velocity Prediction," Geophysical Prospecting, v. 44, p. 687-717.

Zadeh, L.A., 1974: "Fuzzy Logic and Its Application to Approximate Reasoning," Information Processing, 74, 591-594.